UNDERSTANDING THE IMPACT OF PHOSPHORYLATION AND MEMBRANE ON STRUCTURE AND DYNAMICS OF RAS BY MEANS OF MOLECULAR DYNAMICS SIMULATIONS

A THESIS SUBMITTED TO
THE GRADUATE SCHOOL OF
ENGINEERING AND NATURAL SCIENCES
OF ISTANBUL MEDIPOL UNIVERSITY
IN PARTIAL FULFILLMENT OF THE REQUIREMENTS FOR
THE DEGREE OF
MASTER OF SCIENCE
IN
BIOMEDICAL ENGINEERING AND BIOINFORMATICS

By

Metehan İlter

June, 2021

UNDERSTANDING THE IMPACT OF PHOSPHORYLATION AND MEMBRANE ON STRUCTURE AND DYNAMICS OF RAS BY MEANS OF MOLECULAR DYNAMICS SIMULATIONS

By Metehan İlter

18 June 2021

We certify that we have read this dissertation and that in our opinion it is fully adequate, in scope and in quality, as a dissertation for the degree of Master of Science.

Assist. Prof. Dr. Özge Şensoy (Advisor)

Prof. Dr. Canan Atılgan

Assist. Prof. Dr. Nihal Karakaş

Approved by the Graduate School of Engineering and Natural Sciences:

Assoc. Prof. Dr. Yasemin Yüksel Durmaz

Director of the Graduate School of Engineering and Natural Sciences

I hereby declare that all information in this document has been obtained and presented in accordance with the academic rules and ethical conduct. I also declare that, as required by these rules and conduct, I have fully cited and referenced all material and results that are not original to this work.

Signature :

Name, Surname: METEHAN İLTER

ACKNOWLEDGEMENT

First and foremost, I would like to express my deep gratitude to my advisor Dr. Özge Şensoy who has guided me through each step of my research with her great experiences. I must confess that I would not achieve my goals without her support and encouragement.

I am grateful to Tuğçe İnan, Hanife Pekel, and Dilşah Nur Elmacı, who cheered me up whenever I lost my motivation.

I deeply thank all the alumni and current members of Sensoy's Computational Biophysics Lab for making our environment so friendly and warm. I will always be so proud to be a part of such an amazing group.

Finally, I would like to thank my beloved mother Hamide İlter for her endless and unconditional support and encouragement. No words would express my gratitude to her.

This thesis was conducted with the support of TUSEB Computational Structural Biology R & D Project call, reference number: 2019-TA-02-3561.

The numerical calculations reported in this study were performed at TUBITAK ULAKBIM, High Performance and Grid Computing Center (TRUBA resources).

This study is dedicated to my dear father Çetin İlter whose support I feel by my side.

Metehan İlter

June, 2021

CONTENTS

Page

LIST OF FIGURES

LIST OF TABLES

LIST OF SYMBOLS

Cα : Alpha Carbon
Pβ : Beta Phosphate
Pγ : Gamma Phosphate
χ1 : Chi-1 Angle
α3 : Helix-3
L4 : Loop-4

ABBREVIATIONS

RTKs	: Receptor tyrosine kinases
EGFR	: Epidermal growth factor receptor
GRB2	: Growth factor receptor-bound protein 2
GEFs	: Guanine nucleotide exchange factor
GDP	: Guanosine-diphosphate
GTP	: Guanosine-triphosphate
PI3K	: Phosphatidylinositol 3-kinase
MAPK	: Mitogen-activated protein kinase
GAPs	: GTPase-activating proteins
RAS^{WT}	: Wild-type RAS protein
HVR	: Hypervariable region
MD	: Molecular dynamics
PTMs	: Post-translational modifications
FTase	: Farnesyltransferase
ICMT	: Isoprenylcysteine carboxymethyltransferase
DMPC	: 1,2-dimyristoyl-sn-glycero-3-phosphorylcholine
GNP	: Phosphoaminophosphonic acid-guanylate ester
NAMD	: Nanoscale molecular dynamics
VMD	: Visual molecular dynamics
GROMACS	: Groningen machine for chemical simulations
RMSF	: Root-mean-square fluctuation
PCA	: Principal component analysis
RBD	: RAS binding domain
CRD	: Cysteine rich domain

FOSFORİLASYON VE MEMBRANIN RAS YAPISI VE DİNAMİKLERİ ÜZERİNDEKİ ETKİSİNİN MOLEKÜLER DİNAMİK SİMÜLASYONLARIYLA ANLAŞILMASI

ÖZET

Metehan İlter

Biyomedikal Mühendisliği ve Biyoenformatik, Yüksek Lisans

Tez Danışmanı: Dr. Öğr. Üyesi Özge Şensoy

Haziran, 2021

RAS protein ailesi, belirli hücresel sinyal kaskadlarını başlatarak hücre çoğalması, büyümesi, hayatta kalması, göçü ve farklılaşması gibi önemli hücresel fonksiyonların düzenlenmesinden sorumludur. Bu bağlamda, RAS proteinlerinin anormal aktivasyonu, RAS protein ailesinin aracılık ettiği sinyal kaskadlarının aktivasyonunu anormal şekilde tetikleyerek sağlıklı hücrelerin malignitelere dönüşmesine neden olur. Gerçekten de, RAS protein ailesinde görülen aktive edici mutasyonlar, çeşitli kanser türlerine neden olmaktadır. Bu sebeple, RAS protein ailesi, antikanser ilaç geliştirme çalışmalarında sıklıkla hedeflenmektedir. Öte yandan, RAS proteinlerinin sığ yüzeyi ve guanozin trifosfat (GTP) ve guanozin difosfat (GDP) olan endojen ligandların pikomolar bağlanma afiniteleri nedeniyle, protein yüzeyi ile stabil bir şekilde etkileşime girebilen ve klinikte kullanılmaya başlanmış terapötik bir molekül henüz geliştirilmemiştir.. Yıllar geçtikçe, posttranslasyonel modifikasyonların RAS fonksiyonu üzerindeki etkisi aydınlatılmıştır. Özel olarak, tirozin rezidüsünün Src kinaz tarafından fosforillenmesinin H-RAS ve N-RAS izoformlarının RAF'a karşı olan duyarlılığını azalttığı ve kendi içsel GTPaz aktivitesini arttırdığı gösterilmiştir. Fosforillenme, ailenin bir diğer üyesi olan K-RAS4B'nin, içsel GTPaz aktivitesinin azalmasına neden olurken, H-RAS'a benzer olarak, RAF bağlanmasını engellemektedir. Bu tez çalışması kapsamında, yabanıl tip (H-RASWT), H-RASG12D ve K-RAS4BG12D proteinlerinin yapı ve dinamiği ile tirozin rezidüsü üzerinden gerçekleşen fosforillenmenin yabanıl H-RAS ve K-RAS4B (K-RAS4BWT)'ın yapı ve dinamiği üzerindeki etkisi atomistic moleküler dinamik simülasyonları vasıtasıyla incelenmiştir. Daha sonra, moleküler dinamik simülasyonları ile elde edilen mutant proteinlere ait yörüngeler, yörüngelerde, en sık örneklenen konformasyonu belirlemek için kümelenmiştir. Ardından, mutant proteinlerin yapı ve dinamiklerini, fosforillenmiş proteinlerinkine benzetebilen¸ molekülleri tanımlamak için topluluk-tabanlı sanal tarama gerçekleştirilmiştir. Bunun için ZINC15, DrugBank, DrugCentral, BindingDB, NCGC ve CHEMBL veri bankalarından alınan toplamda 33.606 molekül taranmıştır. Sonuç olarak, H-RAS'ın ve K-RAS4B'nin her biri için 10 molekül olmak üzere, toplamda 20 molekülün, mutant proteinlerin dinamik özelliklerini fosforillenmiş proteininkine benzetebildiği gösterilmiştir. Son olarak, hücre zarının mutant proteinlerin su ortamında en sık örneklenen konformasyonlarını da etkileyebileceği gösterilmiştir. Bu sebeple, yakın gelecekte RAS proteinlerinin,

farnesillenmiş ve membrana bağlı halleri gibi ara durumlarının da topluluk-tabanlı sanal taramaya tabi tutulup daha selektif moleküllerin geliştirilebileceği düşünülmektedir.

Anahtar sözcükler: H-RASG12D, K-RAS4BG12D, Src kinaz, RAS-RAF etkileşimi.

UNDERSTANDING THE IMPACT OF PHOSPHORYLATION AND MEMBRANE ON STRUCTURE AND DYNAMICS OF RAS BY MEANS OF MOLECULAR DYNAMICS SIMULATIONS

ABSTRACT

Metehan İlter

MSc in Biomedical Engineering and Bioinformatics

Advisor: Assist. Prof. Dr. Özge Şensoy

June, 2021

The RAS protein family is responsible for regulating paramount cellular functions, such as cell proliferation, growth, survival, migration, and differentiation by initiating certain cellular signaling cascades. With this regard, abnormal activation of the RAS proteins causes the transformation of healthy cells into malignancies by aberrantly triggering the activation of signaling cascades mediated by the RAS protein family. In fact, activating mutations seen in the RAS protein family cause various cancer types. For this reason, the RAS protein family is frequently targeted in studies on the development of anticancer drugs. On the other hand, due to the shallow surface of RAS proteins and picomolar binding affinities of endogenous ligands, which are guanosine-triphosphate (GTP), and guanosine-diphosphate (GDP), a therapeutic molecule that can stably interact with the protein surface and started to be used in the clinic has not yet been developed. Over the years, the effect of post-translational changes on RAS function has been illuminated. Specifically, it was shown that phosphorylation of tyrosine residue by Src kinase attenuates the sensitivity of the H-RAS and N-RAS isoforms towards RAF and increases its intrinsic GTPase activity. While phosphorylation causes a decrease in the intrinsic GTPase activity of K-RAS4B, which is another member of the family, it precludes RAF binding like that of H-RAS. In the scope of this thesis, the structure and dynamics of wild-type (H-RASWT), H-RASG12D and K-RAS4BG12D proteins, as well as the effect of tyrosine phosphorylation on the structure and dynamics of H-RASWT and K-RAS4BWT, were investigated via atomistic molecular dynamics simulations. Thereafter, the trajectories pertaining to the mutant systems obtained by molecular dynamics simulations were clustered to determine the most frequently sampled conformation. Following, ensemble-based virtual screening was performed to identify molecules that can liken the structure and dynamics of mutant proteins to those of phosphorylated proteins. To do so, a total of 33,606 molecules retrieved from the ZINC15, DrugBank, DrugCentral, BindingDB, NCGC, and CHEMBL databases were scanned. Consequently, it was shown that a total of 20 molecules, 10 molecules each for H-RAS and K-RAS4B, could resemble the dynamic properties of mutant proteins to those of phosphorylated proteins. Lastly, it was also shown that the cell membrane could impact the most frequently sampled conformation in the water environment. That is to say, it is thought that in the near future, intermediate states of RAS proteins, such as farnesylated and membrane-bound states,

can also be subjected to ensemble-based virtual scanning to develop more selective ligands.

Keywords: H-RASG12D, K-RAS4BG12D, Src kinase, RAS-RAF interaction.

CHAPTER 1

1. INTRODUCTION

Cancer is attributed to the second leading cause of death in the United States [1]. 19% of cancer cases are known to be led by mutations seen in the RAS protein family. These mutations generally occur at the 12^{th}, 13^{th}, and 61^{st} residues [2], [3]. Consequently, the sensitivity of RAS proteins towards GTPase activating proteins (GAPs) as well as the intrinsic GTPase activity are reduced, whilst the intrinsic nucleotide-exchange activity is enhanced [4], [5]. Among these missense point mutations, the substitution of glycine with aspartic acid at the 12^{th} position is more frequently seen in human beings. In particular, 44% and 39% of colorectal and pancreatic cancers are caused by K-RAS4B^{G12D}, thereby thought of attractive candidate [4], [6]. The same point mutation of H-RAS isoform is highly expressed in ductal carcinoma [7]. In addition, G12D and G12V mutations seen in H-RAS result in resistance to erlotinib in the treatment of head and neck squamous carcinoma [8]. In spite of the fact that H-RAS^{G12D} and K-RAS4B^{G12D} mutants are leading cause of cancer as well as drug resistance, none of the therapeutics have been approved to be prescribed in the clinics yet. The undruggability associated with these mutants has been arisen by the lack of deep pockets on the surface of the isoforms and incapability of competitive binding of inhibitors to the nucleotide-binding pocket [9]–[11]. On the other hand, the extensive effort on developing K-RAS4B^{G12C} mutant protein inhibitors has reached at least clinical trials, thus awakened the hope for the development of RAS inhibitors [12]. Moreover, studies focusing on the RAS allostery have also come into prominence to highlight residues playing in a pivotal role in the function of the protein even though they are distant to the nucleotide-binding pocket [13]. Consequently, over the years, these attempts have brought allosteric modulation of RAS proteins by post-translational modifications (PTMs) into a discussion. From this point of view, recently, the central role of tyrosyl phosphorylation in RAF binding and regulation of the intrinsic GTPase activity have been reported. The phosphorylation of the H-RAS and N-RAS

isoforms at the 32nd position, where a tyrosine resides, ends up with dissociation of RAF as well as an increase in the intrinsic rate of GTP hydrolysis [14]. In line with this, the phosphorylation of the K-RAS4B isoform at the 32nd and 64th positions, where tyrosine residues are found, also results in impairment in the RAF binding, but a decrease in the intrinsic GTPase activity [15]. By courtesy of these outcomes, studies have devoted substantial attention to the possible conformations of Tyr32, which is a well-conserved phosphorylation site for Src-kinase as well as participates in RAF binding. As an example, an experimental study has reported that adaptation of Tyr32 to the out conformation disables the association of H-RAS with RAF, and the binding of GAP is favored as like tyrosyl phosphorylation [16]. For this reason, the conformational selectivity of Tyr32 upon tyrosyl phosphorylation ought to be elaborated and compared with the known conformational states in the literature to provide mechanistic insight into the modulation of RAF and GAP binding. Nevertheless, it is paramount to bear in mind that PTMs of RAS proteins, which take place in the C-terminus of the isoforms, modulate the cellular trafficking of RAS proteins across the distinct cellular compartments[17]. As such, elucidation of the most likely conformations pertaining to RAS proteins in different cellular localizations might widen our perspective for the identification of new possible target sites as well as our perspective to develop more selective RAS inhibitors.

Considering the impact of tyrosyl phosphorylation on RAS-RAF interaction, biasing the mutant RAS proteins towards their phosphorylated forms might allow taking control over the aberrant interaction between RAF and mutant RAS. From this point of view, a holistic understanding of tyrosyl phosphorylation-driven changes in the dynamics and structure of RAS proteins might be an effective strategy for the development of effective therapeutics. In light of these facts, in the scope of this study, we aimed at unveiling conformational changes, which are induced by tyrosyl phosphorylation of H-RAS and K-RAS4B, in particular, tyrosyl phosphorylation-driven by Src kinase, by means of microsecond-long atomistic simulations. Upon the comparison of the systems, namely H-RAS^{G12D}, H-RAS^{WT}, H-RAS^{pY32}, K-RAS4B^{G12D}, K-RAS4B^{WT}, and K-RAS4B$^{pY32,\ pY64}$, the most probable conformations of the mutants were determined and exploited in the ensemble-based virtual screening to repurpose the molecules that could shift the dynamics and structure of the mutant isoforms to those of the phosphorylated proteins. Last but not least, the mutants were also modeled in a 1,2-dimyristoyl-sn-glycero-3-

phosphorylcholine (DMPC) membrane to interrogate the impact of the membrane on the selected reaction coordinates used in the ensemble-based virtual screening.

CHAPTER 2

2. THEORETICAL PART

2.1. The RAS Protein Family and Its Relevance in Tumorigenesis

Ras genes were first discovered as transduced oncogenes in the Harvey and Kirsten sarcoma retroviruses [18]–[20]. After a certain period of time, the presence of these genes in human cancers have also been reported, which then has expedited studies that focus on this gene family and its products [21]. Eventually, over the years, it has been unveiled that RAS proteins, namely H-RAS, K-RAS4A, K-RAS4B, and N-RAS, which are known as small GTPases, mediate cell proliferation, growth, differentiation, and survival [6], [22]–[27]. They act as molecular switches toggling between active and inactive states [28]–[30]. Mechanistically, the phosphorylation status of the nucleotide determines the state of the protein. For activation, the binding of an epidermal growth factor to the extracellular domain of receptor tyrosine kinases (RTKs) leads to dimerization, which, in turn, activates the epidermal growth factor receptor (EGFR). Subsequently, the growth factor receptor-bound protein 2 (GRB2) binds to the phosphorylated tyrosines in the intracellular domain of EGFR towards the SH2 domain. Meanwhile, the SH3 domain of GRB2 recruits RAS-specific guanine nucleotide exchange factors (GEFs) in close proximity to RAS proteins embedded into the plasma membrane [4], [31]. By doing so, dissociation of guanosine-di-phosphate (GDP) from the nucleotide-binding pocket is facilitated, which, in turn, results in binding of highly concentrated guanosine-tri-phosphate (GTP) [30], [32]–[35]. Eventually, in the GTP-bound state, RAS proteins become active, thus being potent in interacting with different effectors, such as RAF, phosphatidylinositol 3-kinase (PI3K), and Ral guanine nucleotide dissociation stimulator that initiate cellular signaling cascades [30], [36], [37]. In this way, cell cycle regulatory proteins are expressed to stimulate cell cycle progression towards mitogen-activated protein kinase (MAPK) signaling. Alternatively, they also trigger anti-apoptotic signaling

towards PI3K/AKT signaling pathway to favor cell survival [4], [38]. On the other hand, upon binding of GAPs, inactivation of this protein family takes place as a result of an increased intrinsic GTPase activity that expedites hydrolysis of GTP to GDP, thus terminating cellular signaling pathways [27], [39], [40].

Considering the signaling cascades regulated by RAS proteins, activating mutations, which attenuate the sensitivity of RAS to GAPs as well as the intrinsic rate of GTP hydrolysis or increase the intrinsic rate of nucleotide exchange are prone to form malignancies since RAS mutants are consecutively active, thus triggering the expression of cell cycle regulatory proteins or anti-apoptotic signaling independent of RTK stimulation [4], [40]. The majority of these missense mutations are clustered at the 12^{th}, 13^{th}, and 61^{st} positions with different prevalence among RAS proteins [3], [41]. 80% of K-RAS mutations occur at the 12^{th} position, whilst 60% of N-RAS mutations are found at the 61^{st} position. Yet, 50% of mutations in H-RAS take place at the 12^{th} position, whereas 40% of the mutations in the same RAS isoform is detected at the 61^{st} position [10]. In addition, mutant isoforms are not inclusive of each other in tumors as each mutant is differently prone to form tumorigenesis in distinct tissues. In parallel to this fact, it has been shown that more than 95% of K-RAS mutants exclusively account for pancreatic cancers, whilst 54% of H-RAS and 94% of N-RAS mutants are known to be responsible for bladder cancers and melanoma, respectively [4], [6], [38]. Nevertheless, wild-type RAS proteins (RAS^{WT}) exist in tumors to enable malignancies. In line with this fact, a K-RAS-driven tumor has been reported together with H-RAS^{WT} and N-RAS^{WT} [30], [42]–[44].

Over the years, several studies have reported that K-RAS mutants are the most frequently detected oncoprotein in several types of adenocarcinomas seen in pancreas, colon, rectum, and lung that are more predominantly stemmed from G12D mutation [2], [27], [45]–[48]. On the other hand, the same mutation in H-RAS is detected in bladder urothelial, infiltrating renal pelvis and ureter urothelial carcinomas, cutaneous melanoma, and colorectal adenocarcinoma, whilst N-RAS^{G12D} is found in acute myeloid leukemia, colon, colorectal, and rectal adenocarcinomas [47].

2.2. Structural Properties of RAS Proteins

The three encoded isoforms of the Ras gene, namely H-RAS, K-RAS4A, and N-RAS, encompasses 189 amino acids, whilst K-RAS4B, which is the splice variant of K-RAS4A,

consists of 188 amino acids. The comparison of the sequences pertaining to isoforms has elucidated that the isoforms share *ca.* 79% sequence identity. Notably, the residues 1-166, which build up the catalytic domain, is highly conserved with a sequence identity rate of almost 89%, whereas the HVR of the isoforms is remarkably variant with an approximately 8% sequence identity rate [27], [49]–[51]. It is also worth mentioning that, unlike the HVR, residues 1-86, namely effector lobe are exactly identical among the isoforms (See **Figure 2.1a**). This invariant region accommodates Switch I (residues 30-38) and II regions (residues 59-76) that actively mediate effector binding (See **Figure 2.1b**) [52]. On the other hand, the allosteric lobe (residues 87-172) is slightly variant (See **Figure 2.1a**) [53], [54]. Notably, this region together with the HVR takes place in the membrane interactions of the isoforms (See **Figure 2.1a**) [55].

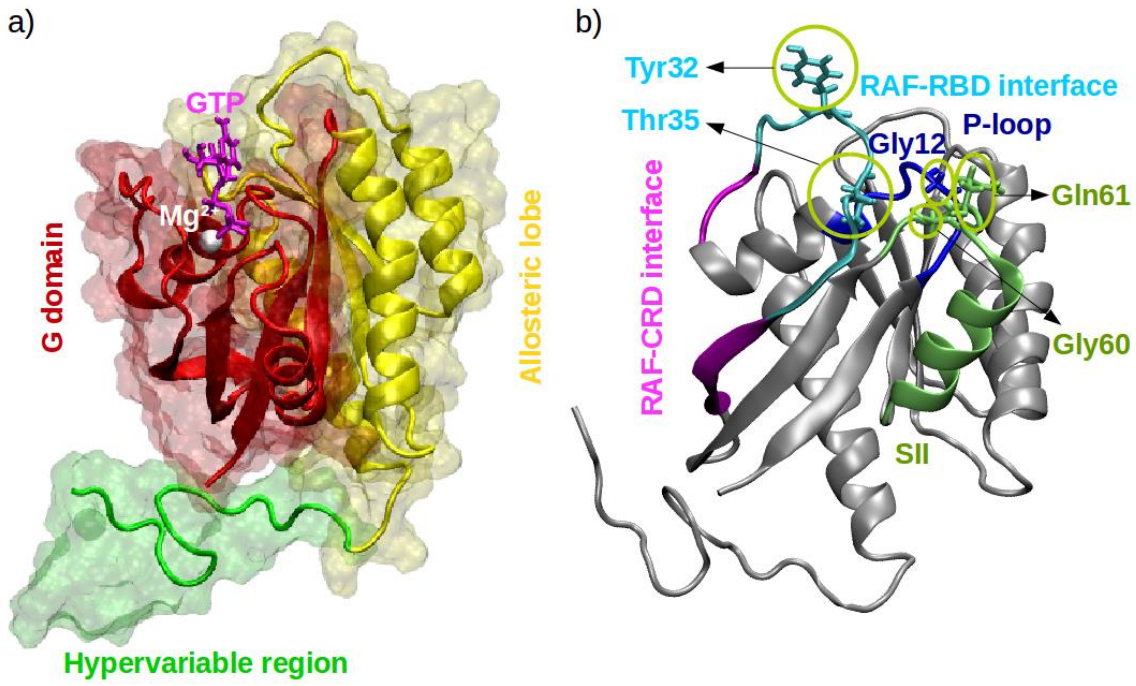

Figure 2.1: a) G domain, allosteric lobe, and hypervariable region of RAS proteins are shown. **b)** Some of the important residues, which are known to be responsible for the function, as well as regions that mediate the interaction of RAS proteins with their effectors are shown.

Moreover, the structural properties of the RAS isoforms, in particular Switch I and II regions, vary on the phosphorylation status of the nucleotide [54], [56]. In detail, Switch I can be found in either open or closed states, namely state 1 and 2, respectively, which, in turn, enable the isoforms to exhibit distinct biochemical activities [57]. When the Switch I region of the isoforms adopts state 1, nucleotide exchange is facilitated, and in parallel to this, effector binding is hindered. On the other hand, upon adoption of Switch

I to state 2, the mobility of Switch II is elevated, which enables cycling between catalytically competent and incompetent states. Furthermore, this conformation drives effector binding to the isoforms that result in further stabilization of Switch I [55], [58].

Considering the fact that most of the human cancers harbor G12 mutations in K-RAS and H-RAS isoforms that display reduced intrinsic or GAP-mediated GTPase activity, structural studies have been conducted to shed some light on the underlying structural causes of these functional alterations [59]–[65]. In addition to structural studies, with the motivation of providing mechanistic insight into the alterations driven by the activating G12 mutations, several molecular dynamics studies have been extensively carried out. Lu *et al.* have reported that G12C, G12D, and G12V mutations seen in K-RAS4B result in a transition from inactive to active conformation by changing dynamics of RAS. Particularly, G12D and G12V mutants of this isoform distorted the nucleotide-binding pocket more in the GTP-bound state than the G12C mutant. On the other hand, the G12C mutant was found to be prone to a more distinguishable conformational change in the GDP-bound state that ascended exposure of the nucleotide [27]. Furthermore, in the scope of another *in silico* study, G12D and G12V mutations seen in H-RAS and K-RAS4B have been comprehensively compared and indicated that G12V mutation increases the flexibility of H-RAS more than that of K-RAS4B and causes H-RAS to adopt a conformation in which it is unable to interact with effectors [66]. Recently, a molecular dynamics (MD) study has uncovered that G12C/V mutations lead to a shift of α3 (residues 87-104) helix further away from loop-7 (residues 105-109). In the same study, it has been shown that these afore-mentioned mutations cause Switch II to be oriented further away from α3 helix and P-loop (residues 10-17) [67].

2.3. Membrane Localization of RAS Proteins

Like GTP-binding, membrane association of RAS proteins is a mandatory factor for their activation so that they can convey cellular signals towards signaling pathways [54], [68]. For this reason, the remarkable keen interest in the activation of the RAS isoforms has prompted cell biology studies that elucidate the membrane localization and cellular trafficking of these proteins across the different cellular compartments. The CAAX motif found in the C-terminal of HVR directs post-translational modifications (PTMs) which mediate the localization of RAS proteins, thus signaling from different cellular compartments [69]–[72]. The HVR region of RAS isoforms undergoes prenylation,

palmitoylation, methylation, and acylation [27], [73]. Yet, the PTMs of the HVR region differ among the isoforms. The Cys pertaining to the HVR of each isoform gets farnesylated. Unlike farnesylation, another Cys residue found in the HVR of H-RAS, K-RAS4A, and N-RAS becomes palmitoylated. These PTMs, indeed, drive the association of the afore-mentioned isoforms with the membrane [74], [75]. On the other hand, in spite of the fact that K-RAS4B does not undergo palmitoylation, it encompasses polybasic Lys motif, which facilitates recruitment of K-RAS4B to the negatively charged membrane [27], [68].

As a more detailed insight into cellular trafficking and membrane localization, the CAAX motif is processed by three enzymes that act sequentially. In the beginning, the unmodified CAAX sequence is the precursor of prenylation by prenyltransferases [76], [77]. Particularly, since the X is not Leu in all the isoforms, farnesyltransferase (FTase) adds 15-carbon farnesyl lipid to the Cys of the CAAX motif [78]. In this way, the modified RAS proteins gain a weak affinity towards cellular membranes [79]. It is also important to emphasize that the only farnesylated RAS protein can accommodate itself on the cytoplasmic face of the endoplasmic reticulum [69]. Subsequently, RAS-converting enzyme 1, which is found on ER, takes action and consequently detaches AAX amino acids [80]. Following this modification, another enzyme entitled isoprenylcysteine carboxylmethyltransferase (ICMT) on endoplasmic reticulum initiates methyl esterification of the alpha-carboxyl group of the farnesylated cysteine [81]. However, all these CAAX modifications are not sufficient to recruit RAS to the plasma membrane unless second signals do not result in further processing of the HVR region. From this perspective, after the modification of the CAAX sequence by the ICMT, the isoforms are directed to the Golgi apparatus. Furthermore, N-RAS possesses one cysteine residue, namely Cys184, that can be palmitoylated, whilst H-RAS harbors two cysteine residues, namely Cys181 and Cys184, that are more prone to palmitoylation. Like N-RAS, only one Cys residue of K-RAS4A, which is Cys180, accepts the palmitoyl group, whereas any cysteine residues of its splicing variant are not palmitoylated [17], [82]. Upon palmitoylation of H-RAS, K-RAS4A, and N-RAS isoforms, they are transported to the plasma membrane. In parallel to this, when these isoforms become depalmitoylated, they are transported back to the cytoplasm [83]. On the other hand, the Lys-rich domain of K-RAS4B, which is positively charged, mediates the binding of K-RAS4B to the plasma

membrane towards electrostatic interactions, which causes dynamic association of this isoform with the plasma membrane [17], [84].

2.4. Druggability of RAS Proteins

RAS mutants account for majority of cancers, thus being spotlighted as attractive targets [85]–[89]. To this end, studies have focused on inhibiting RAS proteins by the nucleotide-binding pocket, RAS-GEF interaction interface as well as RAS-effector interaction interface, and membrane localization [12], [90]–[99]. Albeit remarkable efforts have been spent on developing RAS inhibitors, a small set of molecules could pass the preclinical trials [100], [101]. However, unfortunately, a big slice of this set has not been approved for clinical use. For this reason, RAS proteins are known as undruggable. The undruggability of these proteins is stemmed from the unfeasible competitive inhibitor binding to the nucleotide-binding pocket due to the picomolar binding affinities of GTP/GDP as well as the absence of deep binding cavities on the protein surface alternative to the nucleotide-binding pocket [9]–[11], [102]. In addition to these regions, in the early studies, it has been reckoned that all the RAS isoforms have the same function. In line with this assumption, only H-RAS isoform has been included to develop FTase inhibitors so that membrane interaction of the RAS isoforms might have been occluded [99], [103]. It is also worth mentioning that the therapeutic inefficacy of FTase inhibitors is resulted from alternative lipidation of K-RAS and N-RAS by geranylgeranyltransferase [54], [104]–[106].

Moreover, MD studies have elucidated different conformational states of the nucleotide-binding pocket as well as orientational dynamics of some regions and residues that play a pivotal role in the function of the protein, thus might be exploited as alternative target site [107], [108]. Apart from *in silico* studies, upon mechanistic understanding obtained by experimental approaches, Zn-cyclen and Cu-cyclen compounds were thought of promising to be utilized for the selective targeting of the RAS isoforms to maintain certain conformations of Switch I such as state 1 [13], [56], [109]. Yet, these attempts were not sufficient to pose therapeutics beyond *in vivo* studies. In another recent study, orientational dynamics of H-RAS^{G12P} and H-RAS^{G12D}, which are, in seriatim, non-transforming and transforming mutants, have been compared and reported that Tyr32 displayed distinct dynamics. Particularly, Tyr32, which regulates RAF binding and intrinsic GTPase activity, was more exposed in the non-transforming mutant. For this

reason, Tyr32 was concluded as a promising residue that needs to be targeted with small molecules to invoke dynamics properties in H-RAS^{G12D}, which are more similar to those of H-RAS^{G12P} [108].

Furthermore, more interestingly, a study has shown that the substitution of Gly at the 12th position with Cys has ended up with the formation of a pocket, namely P2 pocket, in the GDP-bound state of RAS. Eventually, this has shifted research towards the development of mutant-specific covalent inhibitors that can bind with Cys residue [110]–[113]. Following this study, the first covalent K-RAS4B^{G12C} inhibitor entitled AMG 510 has successfully passed preclinical studies, and subsequently, its clinical studies have been started (clinicaltrials.gov identifier NCT03600883) [100], [114], [115]. However, the undruggability issue of K-RAS4B for its other mutants as well as mutations seen in other isoforms has remained an enigma for the treatment of cancers.

2.5. Src Kinase-mediated Tyrosyl Phosphorylation of RAS Proteins

Phosphorylation as a post-translational modification regulates the function of the proteins [116]. The cellular RAS proteins cannot undergo autophosphorylation but require kinases to get phosphorylated [117]–[119]. In particular, Tyr4, Tyr32, Tyr64, Tyr137, Ser89, Ser181, Thr144, and Thr148 are well-known residues that undergo phosphorylation [14], [15], [99], [120]–[124]. On the other hand, viruses can phosphorylate their RAS protein [117]–[119]. Recently, tyrosyl phosphorylation, which is mediated by Src-kinase, has come into prominence in the literature, since it substantially alters the intrinsic rate of GTP hydrolysis and RAS-RAF interaction [14], [15], [125].

Src is one of the oncogenes which controls cell growth, proliferation, survival, and migration [99], [126]. In the course of time, with the knowledge of its relevance in cancer, the impact of Src-kinase on RAS proteins has been deeply scrutinized. Bunda *et al.* have reported that Src kinase can phosphorylate tyrosine at the 32nd position of GTP-bound H-RAS and N-RAS, which, in turn, causes an increase in the rate of intrinsic GTP hydrolysis and impairment of RAF binding to the mentioned isoforms. In the same study, it has been also proposed that the phosphoryl group of tyrosine repels the negatively charged Asp38 and Asp57, thus changing either conformation or position of Switch I in such a fashion that RAF binding is occluded. In parallel to this, this electrostatic repulsion facilitates the exposure of Tyr32, which might be prone to break down the critical hydrogen bond between the hydroxyl group of Tyr32 and Pγ of GTP, thus potentiating more efficient

hydrolysis of GTP via nucleophilic water attacks [14]. Interestingly, in a recent MD study, it has been shown that the increased rate of GTP hydrolysis pertaining to H-RAS^{G12P}, namely non-transforming mutant, was correlated to the eradication of the mentioned hydrogen bond. In this way, Tyr32 was more likely to be found distant to the nucleotide-binding pocket. Indeed, considering the spatial organization of Tyr32, the change in the orientation of this residue might elevate the accessibility of GTP to nucleophilic water attacks [108]. In another study, it has been unveiled that SHP2 can dephosphorylate the phosphorylated Tyr32 pertaining to either H-RAS or N-RAS, and consequently, enable these isoforms to interact with RAF, thereby initiating signal transduction through the relevant pathway [99], [127]. In a recent study, it has been reported that Tyr32 and Tyr64 of K-RAS4B can be phosphorylated by Src kinase, which alters the conformational state of Switch I and II. More significantly, the phosphorylation of these residues reduced both GAP-mediated and intrinsic GTPase activities as well as GEF-mediated nucleotide exchange activity. Conversely, the intrinsic rate of nucleotide-exchange was increased, thus keeping K-RAS4B in a GTP-bound state. Nevertheless, the tyrosyl phosphorylation concurrently stalled RAF binding to K-RAS4B, and, for this reason, it decoupled from the corresponding signaling pathway. Like H-RAS and N-RAS isoforms, in the same study, it has been shown that the tyrosyl phosphorylation of K-RAS4B could be reversed by SHP2 [15]. In line with this experimental study, a contemporary *in silico* study has indicated that the afore-mentioned tyrosyl phosphorylation of K-RAS4B, indeed, alters the conformational state of the nucleotide-binding pocket. In particular, in the GDP-bound state, the volume of the nucleotide-binding pocket was extended. Subsequently, this conformational change was exploited to interpret the increased rate of the intrinsic nucleotide change. In addition, at the borderline of the previous experimental study, this study has elucidated that tyrosyl phosphorylation shifts the favorable conformation of K-RAS4B towards an unfavorable conformation for both GAP and GEF binding. Last but not least, in the same study, it has been reported that the allosteric propagation pathway from the RAS-RAF interface to the L4 loop of RAF that is known to be responsible for RAF kinase activation was disturbed as a result of tyrosyl phosphorylation [128]–[130].

Considering the pivotal role of tyrosyl phosphorylation in RAF binding as well as regulation of the intrinsic GTPase activity, a holistic understanding of tyrosyl phosphorylation and invoking dynamics and structural properties in mutant RAS proteins,

which resemble those of the phosphorylated system, might be an effective strategy for the development of effective therapeutics.

CHAPTER 3

3. EXPERIMENTAL PART

3.1. System Setup Pertaining to Cytosolic States of the Proteins for Molecular Dynamics Simulations

The atomistic MD simulations were performed for GTP-bound (i) H-RAS^{WT} (PDB ID: 5P21), (ii) H-RAS^{G12D} (PDB ID: 1AGP), (iii) H-RAS^{pY32} (PDB ID: 5P21), (iv) K-RAS4B^{WT} (PDB ID: 3GFT), (v) K-RAS4B^{G12D} (PDB ID: 4DSN), and (vi) K-RAS4B$^{pY32,\ pY64}$ (PDB ID: 3GFT), whose crystal structures were downloaded from the Protein Data Bank (https://www.rcsb.org/) [60], [131]–[134]. For the preparation of the GTP-bound H-RAS^{WT}, H-RAS^{G12D}, and H-RAS^{pY32}, the phosphoaminophosphonic acid-guanylate ester (GNP)-bound crystal structures were converted into GTP-bound forms by exchanging the N_3B atom with an oxygen atom. After this modification, GTP-bound H-RAS^{WT} and H-RAS^{G12D} were protonated at pH 7.4 according to the obtained pKa values from the ProPka server [135], [136]. For the phosphorylated H-RAS system, namely H-RAS^{pY32}, Tyr32 was patched with TP2 phosphoryl groups by considering its calculated pKa value pertaining to H-RAS^{WT} [137]. Furthermore, for the preparation of GTP-bound K-RAS4B^{WT}, the GNP was converted into GTP as described above and the citric ion present in the crystal structure was removed. Following these changes, His61 was mutated back to Gln. Finally, the prepared system was protonated at pH 7.4 as it was done for the H-RAS systems. For the phosphorylated K-RAS4B system, K-RAS4B$^{pY32,\ pY64}$, the TP2 phosphoryl group was added to Tyr32 and Tyr64. Lastly, for GTP-bound K-RAS4B^{G12D}, the C_3B atom of phosphomethylphosphonic acid-guanylate ester was substituted with an oxygen atom and the 1,2-ethanediol existed in the crystal was removed. Afterwards, Ser1 was reverted to Met1. Eventually, the modified system was protonated under the same conditions for the afore-mentioned systems.

The GTP-bound H-RAS^{WT}, H-RAS^{G12D}, and K-RAS4B^{G12D} systems were solvated with 9 Å water thickness, whereas 15 Å water layer thickness was set for the rest of the systems. As a side note, the TIP3P water model was utilized [138]. Following the solvation of each system, the systems were neutralized with 0.15 M NaCl.

3.2. Simulation Protocol of the Cytosolic Systems

MD simulations of the cytosolic proteins were performed via Compute Unified Device Architecture version of Nanoscale Molecular Dynamics (NAMD) that enables the use of graphical processing units [139]. The systems were modeled according to the CHARMM36 force-field [140]–[144]. The pressure, temperature, and time step were adjusted as, in seriatim, 310 K and 1 atm, 2 femtoseconds (fs). The set cut-off value of non-bonded interaction was 12 Å, whilst the long-range electrostatic interactions were calculated utilizing particle mesh Ewald [145], [146]. In the end, the systems were minimized for 4.8 picoseconds (ps), and subsequently, simulated for a total of ca. 13.5 microseconds (μs) in the NPT ensemble. It is also crucial to stress that each simulation was performed with two replicates whose initial velocities were different.

3.3. Molecular Dynamics Simulations of GTP-bound H-RAS^{G12D} and K-RAS4B^{G12D} in DMPC Membrane

The retrieved crystal structure of H-RAS^{G12D} (PDB ID: 1AGP) and K-RAS4B^{G12D} (PDB ID: 4DSN) were utilized for the membrane systems [60], [132]. The GTP-bound states of the systems were prepared as defined above. The HVR region of the H-RAS system was modeled by aligning the crystal structure of the G12D mutant to the crystal structure of H-RAS^{G12V} (PDB ID: 2Q21) [147]. By doing so, the residues 166-171 were modeled. The rest of the residues were included in the model by means of the 'Build Peptide From Sequence' module of Schrödinger [148]. Thereafter, the PTMs were introduced to the prepared system via the 'Solution Builder' of CHARMM-GUI, where the system was also prepared for the MD simulations [149]–[151]. In detail, Cys181 and Cys184 were modified with a palmitoyl group, whereas a farnesyl group was added to the Cys186. In addition to palmitoylation and farnesylation of Cys residues, the C-terminal was capped with the CT1 that corresponds to the addition of a carboxymethyl group to the backbone. Subsequently, the modified system was solvated and neutralized with 22 Å of a water layer thickness and 0.15 M NaCl, respectively. The neutralized system was simulated under the same conditions with the cytosolic states to equilibrate the model structure. The

equilibrated model was embedded into a DMPC (1:1) membrane model by aligning the first principle axis along the z-direction and translating the protein along the negative direction of the same axis by 42 Å. For this, the 'Membrane Builder' of CHARMM-GUI was utilized and obtained files from the servers were made use of performing MD simulation with exactly the same conditions as those of the cytosolic systems (See **Figure 3.1a**) [149], [151]–[155]. The membrane-bound H-RAS^{G12D} was simulated for a total of 0.680 μs in three replicates.

In the same way with the membrane bound-H-RAS^{G12D} system, the membrane-bound state of the K-RAS4B mutant was prepared. In detail, the first 180 residues of K-RAS4B^{G12D} were crystallized in the retrieved PDB file. Hence, the rest of the residues were modeled using the 'Build Peptide From Sequence' module of Schrödinger [148]. After filling the missing atoms in the side-chain with the Prime, farnesyl, and carboxymethyl groups were added to the Cys185 and C-terminal, respectively via the 'Solution Builder' of CHARMM-GUI [149]–[151], [156], [157]. The modified system was solvated and neutralized with, in seriatim, 12 Å water layer thickness and 0.15 M NaCl. Afterwards, the system was equilibrated by running an MD simulation with exactly the same system set up as those of the cytosolic system for 100 ns. The equilibrated system, then, was inserted into a DMPC (1:1) membrane, which was established by 'Membrane Builder' of the CHARMM-GUI, by aligning the first principle axis along the z-direction and translating the aligned protein along the -z-direction by 45 Å (See **Figure 3.1b**) [149], [151]–[155]. MD simulations of membrane-bound K-RAS4B^{G12D} were performed for a total of almost 0.8 μs in two replicates.

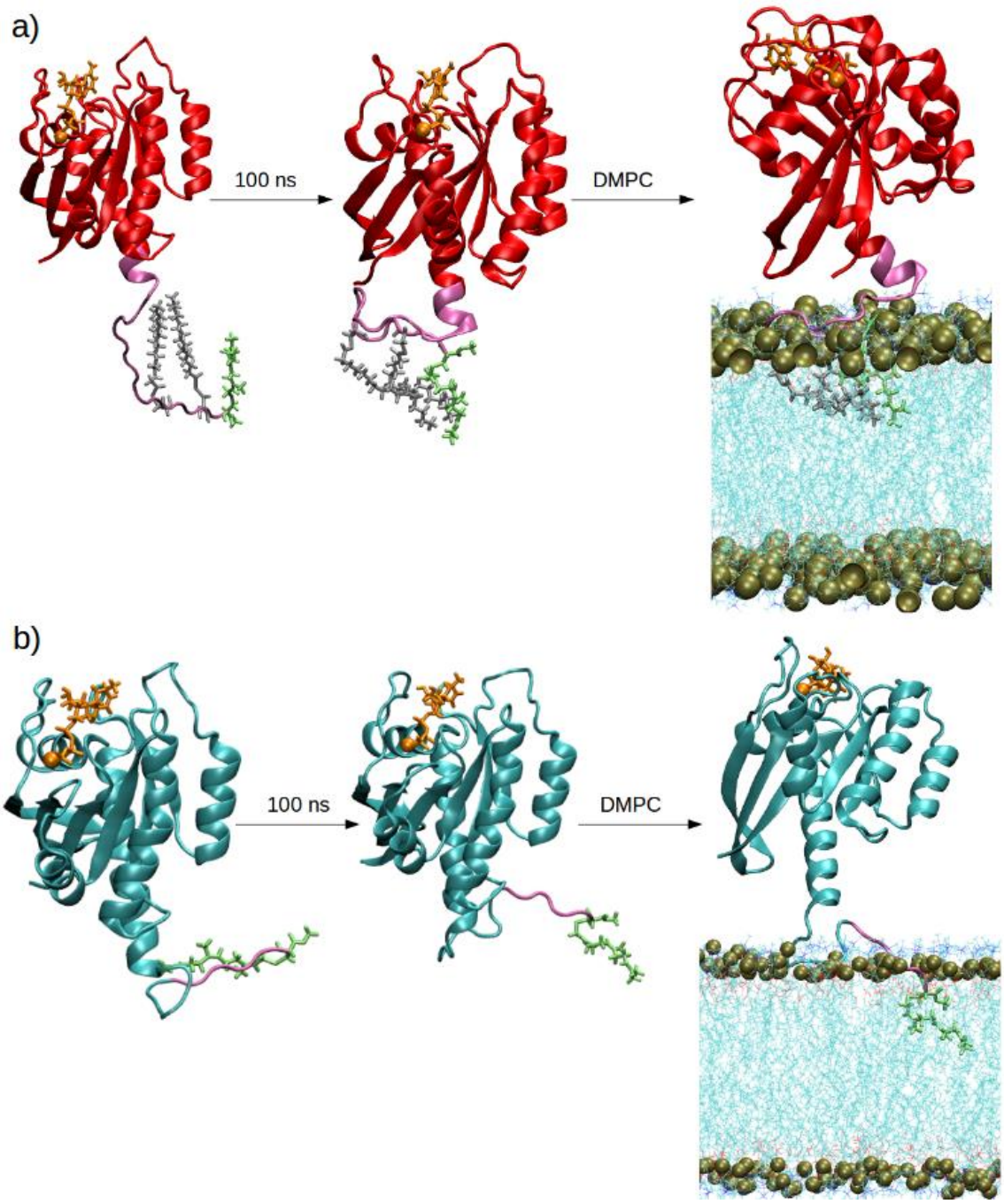

Figure 3.1: The modeling of the HVR region along with PTMs as well as an equilibration of the model structures for burying the **a)** H-RAS^{G12D}, and **b)** K-RAS4B^{G12D} systems into a DMPC membrane model.

3.4. Ensemble-based Virtual Screening

3.4.1. Clustering of conformations sampled in the H-RAS^{G12D} and K-RAS4B^{G12D} trajectories

The conformational states of the nucleotide-binding pocket pertaining to the mutant H-RAS and K-RAS4B were clustered based on the distance (i) between the side-chain oxygen of Thr35 and Pβ of GTP, (ii) between the backbone amide of Gly60 and Pβ of

GTP, and (iii) between the side-chain oxygen of Gln61 and Pβ of GTP throughout the obtained trajectories. Upon selection of the representative frames pertaining to different conformational states of the mutants, the structures were prepared for the 'SiteMap' module of Schrödinger to identify plausible binding pockets on the protein surface [148], [158], [159]. To this end, GTP and Mg^{2+} were removed from the representative structures, and subsequently, the proteins were optimized in OPLS3e force-field using the 'Protein Preparation' module of Schrödinger [148], [160], [161]. The optimized structures were utilized as inputs for the 'SiteMap' module, which, in turn, gave SiteScore values for possible binding cavities on the protein surfaces [148], [158], [159]. In the end, the pocket having the highest SiteScore value among the other possible ones was selected to be used for further steps of this study.

3.4.2. Determination of pharmacophore groups pertaining to binding sites identified and searching molecules in ligand databases

Pharmacophore features pertaining to binding sites in the mutant systems were elucidated using the chemical and geometrical properties of the residues 29-34 via the 'Develop Pharmacophore Model' module of Scrödinger [162], [163]. Following, ligands were downloaded from the ZINC15 [164]–[166], DrugCentral [167]–[169], NCGC [170], BindingDB [171]–[174], and DrugBank [175]–[178] databases. Molecules having at least 3 pharmacophore matches and a molecular weight of less than 550 kDa were filtered out using the 'Ligand Filtering' module of Scrödinger [148].

3.4.3. Molecular docking of the ligands to the identified cavities of the H-RAS^{G12D} and K-RAS4B^{G12D} proteins

Grid boxes of the mutant systems were determined according to the centroid of the residues 29-34, which build up the binding pocket, by means of the 'Receptor Grid Generation' module of Scrödinger [148], [179]–[181]. This enables to calculate the interactions between the ligands and identified pocket. Before the molecular docking, the ligands were primed using the 'LigPrep' module of Scrödinger based on OPLS3e force-field [148], [161]. Subsequently, each candidate molecule was docked to the cavity of the corresponding mutant utilizing the 'Standard-Precision (SP)' algorithm of the 'Glide' [148], [179]–[181]. The docked ligands to the cavities were assessed according to their GScores as well as orientations with respect to the nucleotide-binding pocket. Poses having an orthogonal orientation towards the nucleotide-binding pocket and relatively lower GScore were thought of promising.

3.4.4. Molecular dynamics simulations of ligand-H-RAS^{G12D}/K-RAS4B^{G12D} complexes

Following the determination of the promising candidates based on their GScore values and orientations, their impacts on the structural and dynamical properties of H-RAS^{G12D}/K-RAS4B^{G12D} were investigated by means of atomistic simulations. With this regard, the topology and parameter files pertaining to the ligands of interest were obtained from the 'Ligand Reader & Modeler' of CHARMM-GUI [149], [182]. Thereafter, the ligand-protein complexes were protonated under the same conditions as those of the other systems. The protonated complexes were solvated and neutralized with 15 Å of water layer thickness and 0.15 M NaCl, respectively. MD simulations of each complex were performed as least-wise two replicates, and, the complexes were simulated for a total of 44.048 μs.

3.5. Trajectory Analysis

Each replicate of the systems was concatenated and visualized in the 'Visual Molecular Dynamics (VMD)' software, where representative figures were generated using the 'Taychon Render' [183], [184]. The local and global features of the systems studied were illuminated using the 'Groningen Machine for Chemical Simulations (GROMACS)' [185], [186].

3.5.1. Root-mean-square fluctuation

The root-mean-square fluctuation (RMSF) profiles of backbone atoms were elucidated over the course of the obtained trajectories by making use of the 'gmx rmsf' module of GROMACS, where the module solved the following formula (See **Equation 3.1**) [185], [186].

$$RMSF = \sqrt{\frac{1}{T}\sum_{t=1}^{N}(B_i(t) - \widetilde{Bi})} \quad \textbf{(3.1)}$$

, where the duration of the simulation and coordinates of backbone atom at time t are denoted by T and $B_i(t)$, respectively.

In light of the above-mentioned formula, the fluctuation of each residue was computed, which provided a holistic insight into the dynamics of the systems studied. In addition, the impacts of the ligands on the stability of the region that mediates RAF binding were investigated by subtracting the backbone RMSF value of the region pertaining to ligand-H-RAS^{G12D}/K-RAS4B^{G12D} from that of H-RAS^{G12D}/K-RAS4B^{G12D}.

3.5.2. Probability distribution of the measured distances between the certain reaction coordinates

The distance between the certain reaction coordinates was measured over the course of the trajectories using the 'gmx distance' module of GROMACS [185], [186]. Thereafter, the obtained time-line data was converted into probability plots. To do so, the minimum and maximum sampled distances within computed raw data were determined, and with this regard, the frequency of each interval was determined by setting the sampling range to 2 Å. As a side note, the frequency interval was adjusted as 1 Å for more sensitive and accurate the selection of representative frames for the ensemble-based virtual screening. In the end, the frequency of each range was divided by the number of data points, which in turn, gave the probability distribution of the Tyr32, which reflects its exposure. By doing so, the impact of tyrosyl phosphorylation, as well as repurposed molecules on dynamic and structural properties of H-RAS^{G12D}/K-RAS4B^{G12D}, were deciphered.

3.5.3. Probability distribution of the side-chain torsions of Tyr32

The side-chain torsion angle of Tyr32, namely χ1, was measured over the course of trajectories pertaining to the K-RAS4B systems by use of the VMD [183]. Then, the frequency of each sampling range was calculated, where the sampling range was adjusted to 10 degrees. In the end, the frequency of each range was divided by the number of data points, which in turn, gave the probability of the Tyr32 being found at a certain position that reflects its exposure.

3.5.4. Essential dynamics analysis

As a global investigation of the obtained trajectories, principal component analysis (PCA) was carried out to uncover collective motion taking place in the trajectories, which shed some light on distinctions and similarities in dynamic properties of the systems studied, in particular in the mutant and phosphorylated systems. According to this unsupervised machine learning approach, the Cα atom of each residue was selected, and picked up atoms were aligned to the initial frame over the time of trajectory. Then, covariance matrices of each system were generated and diagonalized (See **Equation 3.2**).

$$C_{zk} = \langle M_{zk} \Delta r_z \Delta r_k \rangle \quad \textbf{(3.2)}$$

, where a change in the position of each coordinate of z and k atoms is indicated by $M_{zk}\Delta r_z \Delta r_k$, which gives a C_{zk}, namely a co-variance matrix.

Right after the diagonalization, eigenvectors and eigenvalues of each system were calculated from the corresponding covariance matrix of the system of interest (See **Equation 3.3**).

$$diag(C_{zk}) = \delta\vartheta^2 \quad \textbf{(3.3)}$$

, where the obtained eigenvector and values pertaining to a diagonalized covariance matrix are obtained by ʊ and δ^2, respectively.

The generation and diagonalization of co-variance matrices, as well as the calculation of eigenvectors and eigenvalues from the diagonalized covariance matrices, were achieved with the help of the 'gmx covar' module of GROMACS. The projection of trajectories with respect to the eigenvector of interest as well as cumulative fluctuation of each residue throughout the trajectories were achieved by the use of the 'gmx anaeig' module of GROMACS [185], [186].

CHAPTER 4

4. RESULTS AND DISCUSSION

In the scope of this thesis, dynamic and structural properties of GTP-bound H-RAS^{WT}, H-RAS^{G12D}, H-RAS^{pY32}, K-RAS4B^{WT}, K-RAS4B^{G12D}, and K-RAS4B$^{pY32,\ pY64}$ were comprehensively compared by performing atomistic MD simulations. In this way, the structural and dynamical changes driven by either tyrosyl phosphorylation or G12D mutation were elucidated. Moreover, a novel binding pocket next to the nucleotide-binding site was identified on the surface of the mutant systems. By courtesy of the mechanistic understanding, several drug libraries were scanned to identify small molecules that could resemble dynamic and structural properties of the phosphorylated systems in the G12D mutant systems. Consequently, a total of 20 molecules, 10 per mutant, were identified as promising which can invoke similar dynamics and structural features in the mutant systems that are similar to those of the phosphorylated system. Last but not least, the impact of the DMPC membrane model on the key regulatory residue Tyr32 and reaction coordinates, which were used for clustering the trajectories, were investigated. With this regard, it was shown that the membrane altered the conformational state of the nucleotide-binding pocket pertaining to H-RAS^{G12D} and K-RAS4B^{G12D}. These uncovered distinctions might be taken into account for developing more selective therapeutics that target the RAS proteins based on their cellular localization.

4.1. The Comparison of RMSF Profiles Showed Considerable Differences in the Residues with Important Function

The obtained backbone RMSF values throughout the trajectories of the systems studied highlighted significant changes arisen by substitution of Gly with Asp at the 12th position and tyrosyl phosphorylation.

In H-RAS isoform, upon tyrosyl phosphorylation taking place at the 32nd position as well as the above-mentioned mutation, the mobility of the residues 30-40 that interact with the

RAF-RAS binding domain (RBD) was substantially increased [129]. In the same manner, the fluctuation of the residues 27-29 and 41-45, which mediate RAF-cysteine rich domain (CRD) interaction, were remarkably increased as a consequence of the tyrosyl phosphorylation. However, interestingly, these residues were not highly fluctuating over the time of MD trajectories pertaining to the H-RAS^{WT} and H-RAS^{G12D} systems, which might enable RAS-RAF interaction (See **Figure 4.1a**) [129]. Considering the fact that phosphorylation of H-RAS by Src kinase unable RAF recruitment, the concurrent increased mobility of the residues that are involved in RAF-RBD and -CRD interactions might pose this incapability [14]. For this reason, increasing the fluctuation of these regions in the mutant system via small therapeutics might occlude H-RAS-RAF interaction. Furthermore, Tyr32, which is located on the Switch I region, fluctuated more in the mutant and phosphorylated systems compared to the wild-type protein (See **Figure 4.1a**). However, it is worth mentioning that the elevation in the fluctuation of Tyr32 explored in the phosphorylated system was considerably higher than that of the mutant system (See **Figure 4.1a**), which might facilitate this residue to adopt different conformational states that may not be sampled by the mutant system, as elucidated in our recent *in silico* study [108]. More significantly, Bunda *et al.* have also reported that the H-RAS^{pY32} displayed higher intrinsic GTPase activity than its unphosphorylated counterparts [14]. With this regard, the increased fluctuation of Tyr32 might be related to the enhanced intrinsic GTPase activity as if the phosphorylation makes Tyr32 exposed, which, in turn, might promote nucleophilic water attacks to Pγ of GTP. With these formerly discussed facts, unlike the significant alteration in the mobility of Switch I, which entirely includes residues that are involved in the RAF-RBD interaction, the Switch II region, in general, was drastically affected by neither mutation nor tyrosyl phosphorylation (See **Figure 4.1a**). Nevertheless, as an exception, the mobility of the catalytically important residue Gln61 showed an increase as a result of the tyrosyl phosphorylation (See **Figure 4.1a**). Considering the catalytic importance of this residue and the functional influence of tyrosyl phosphorylation on H-RAS, this increase might prompt the shift of H-RAS towards the catalytically competent state [13], [58], [187].

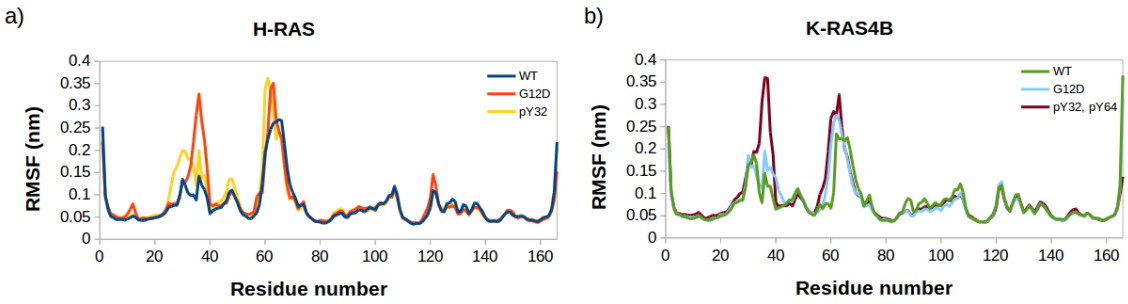

Figure 4.1: The backbone RMSF of the GTP-bound **a)** H-RAS^{WT}, H-RAS^{G12D}, and H-RAS^{pY32}, and **b)** K-RAS4B^{WT}, K-RAS4B^{G12D}, and K-RAS4B$^{pY32,\ pY64}$ systems were computed from the concatenated trajectories.

As opposed to the abrupt increase in the mobility of the residues mediating RAF-RBD interaction in H-RAS^{G12D}, the same mutation in the K-RAS4B isoform slightly elevated the flexibility of the same residues (See **Figure 4.1b**). On the other hand, a drastic fluctuation of these residues in K-RAS4B was highly driven by the tyrosyl phosphorylation. However, the flexibility of the residues 27-29 and 41-45 playing a key role in RAF-CRD interaction in K-RAS4B was not affected by either mutation or phosphorylation. Moreover, Tyr32 pertaining to K-RAS4B^{G12D} fluctuated less than that of K-RAS4B^{WT}, whilst the flexibility of this residue went up upon the tyrosyl phosphorylation (See **Figure 4.1b**). Since K-RAS4B$^{pY32,\ pY64}$ shows attenuated intrinsic GTPase activity and is incapable of interacting with RAF, increasing the flexibility of the residues controlling RAF-RBD interaction in the K-RAS4B^{G12D} system might be a promising strategy to achieve a therapeutic effect by terminating the relevant signaling pathway [15]. Besides the mutation or tyrosyl phosphorylation-driven changes in the fluctuation pattern of the residues that predominantly control RAF binding, the Switch II region of the same isoform systems was also compared. The comparison highlighted that the Switch II region of K-RAS4B$^{pY32,\ pY64}$ fluctuated the most, whereas the same region of K-RAS4B^{G12D} slightly fluctuated compared to K-RAS4B^{WT} (See **Figure 4.1b**). Furthermore, Gln61 of both K-RAS4B^{G12D} and K-RAS4B$^{pY32,\ pY64}$ were more flexible than that of K-RAS4B^{WT}, where that of the latter was the most flexible (See **Figure 4.1b**).

4.2. Src Kinase-mediated Tyrosyl Phosphorylation Could Considerably Change the Orientational Dynamics of Tyr32

Tyr32 of H-RAS and Tyr32/Tyr64 of K-RAS4B isoforms are known to undergo phosphorylation driven by Src kinase. The impact of this phosphorylation on the function of H-RAS isoform has been reported as an increase in the intrinsic rate of GTP hydrolysis

and stalled RAF binding [14]. Furthermore, like H-RAS^{pY32}, K-RAS4B$^{pY32,\ pY64}$ is not able to interact with RAF [15]. However, as opposed to the increased intrinsic rate of GTP hydrolysis observed in H-RAS^{pY32}, the double phosphorylation of K-RAS4B causes loss of the intrinsic GTPase activity [15]. By taking encouragement from the significance of Tyr32 for the regulation of both intrinsic GTPase activity and RAF binding, its orientational dynamics was scrutinized by measuring the distance between the side-chain oxygen of Tyr32 and Pβ of GTP. In light of the trajectory analysis, it was shown that Tyr32 of H-RAS^{G12D} was more likely to be found in the vicinity of the nucleotide-binding pocket as like that of RAF-RBD-bound H-RAS^{WT}, whereas that of H-RAS^{pY32} placed itself outward of the nucleotide-binding pocket like H-RAS^{G12P} (See **Figure 4.2a** & **4.2b**) [108]. In parallel to the anticipations, Tyr32 of H-RAS^{pY32} was more likely to be exposed like that of H-RAS^{G12P}, whereas the same residue of H-RAS^{G12D} was not exposed. The exposure of Tyr32 might, indeed, facilitate the nucleophilic water attacks to the Pγ of GTP, which, eventually, turns GTP into GDP. This finding also suggests an explanation for the increased intrinsic GTPase activity upon the tyrosyl phosphorylation.

Both the tyrosyl phosphorylation and G12D mutation pertaining to the K-RAS4B isoform caused an increase in the sampled distances between the aforementioned atom-pairs. More importantly, even though K-RAS4B^{G12D} sampled slightly longer distances than K-RAS4B$^{pY32,\ pY64}$, Tyr32 of the mutant was not exposed, whereas that of the phosphorylated K-RAS4B was more prone to be found exposed as explored by the measured χ1 angle over the course of trajectories (See **Figure 4.2c**, **4.2d**, **4.2e**, and **4.2f**). This might be explained by the repulsion of the negatively charged phosphoryl group patched to Tyr32 by the negatively charged nearby residues. From this point of view, it might be concluded that even the slight and constant repulsion of Tyr32 away from the nucleotide-binding pocket would be enough to occlude RAF binding with the help of the electrostatic interactions (See **Figure 4.2d**). It is also important to bear in mind that exposure of Tyr32 in K-RAS4B^{G12D} might be achieved by a vast increase in the mentioned sampled distance. Last but not least, yet, this slight change may not be enough to expedite the intrinsic GTPase activity due to the incapability of the tyrosyl phosphorylation to considerably ascend the accessibility of GTP to the nucleophilic water attacks. Even worse, the bulky phosphoryl group may prevent these attacks and culminate in the loss of this activity as shown in a recent study [15].

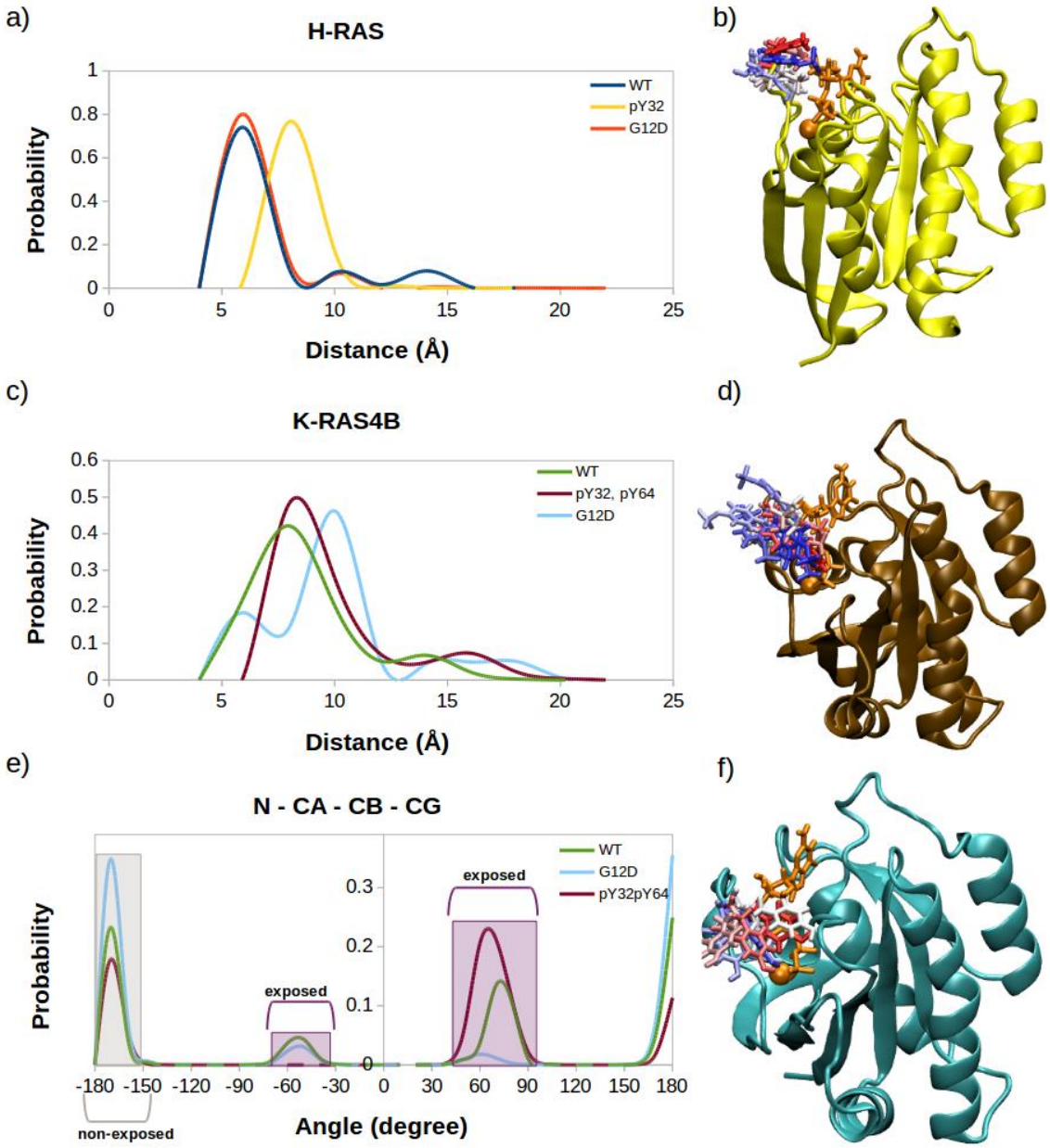

Figure 4.2: a) The probability distribution of the distance measured between the side-chain oxygen atom of Tyr32 and Pβ atom of GTP over the course of trajectories pertaining to H-RAS^{WT}, H-RAS^{pY32}, and H-RAS^{G12D}. **b)** The orientational dynamics of Tyr32, which was colored with respect to the time-step and shown in the licorice representation, throughout the obtained trajectories of H-RAS^{pY32}. **c)** The probability distribution of the distance measured between the side-chain oxygen atom of Tyr32 and Pβ atom of GTP over the course of trajectories pertaining to K-RAS4B^{WT}, K-RAS4B$^{pY32, pY64}$, and K-RAS4B^{G12D} systems. **d)** The orientational dynamics of Tyr32, which was colored with respect to the time-step and shown in the licorice representation, throughout the obtained trajectories of K-RAS4B$^{pY32, pY64}$. **e)** The probability distribution of the side-chain torsion of Tyr32 pertaining to the K-RAS4B systems. **f)** The orientational dynamics of Tyr32, which was colored with respect to the time-step and shown in the licorice representation, throughout the obtained trajectories of K-RAS4B^{G12D}.

4.3. Principal Components of the Systems Studied Showed That Local Dynamic Properties Are Consistent with Collective Motions

In addition to the comparison of local dynamic properties, the collective motion taking place in the obtained trajectories of the systems was also investigated with the help of essential dynamics analysis. To this end, the eigenvalues and eigenvectors of each system were calculated and the projection of trajectories along the first three eigenvectors was taken, which almost account for almost 50% of overall dynamics. From this perspective, the point mutation and tyrosyl phosphorylation of H-RAS caused a remarkable overall change in the Switch I and II regions (See **Figure 4.3a** and **4.3b**), which is in line with the observed RMSF values of the same systems. As a closer look into this conclusion, it is important to stress that the contribution of the residues, which are important for H-RAS-RAF-CRD interaction, was higher in the H-RAS^{pY32} system than that of the mutant systems. As opposed to the previous finding, the residues that mediate H-RAS-RAF-RBD interaction in H-RAS^{pY32} had lower contributions to the collective dynamics than those of H-RAS^{G12D} (See **Figure 4.3a**). Furthermore, like the local observations, the impact of the tyrosyl phosphorylation on the global dynamics pertaining to the Switch II region, in particular, Gln61, was relatively more than that of the mutant (See **Figure 4.3a**).

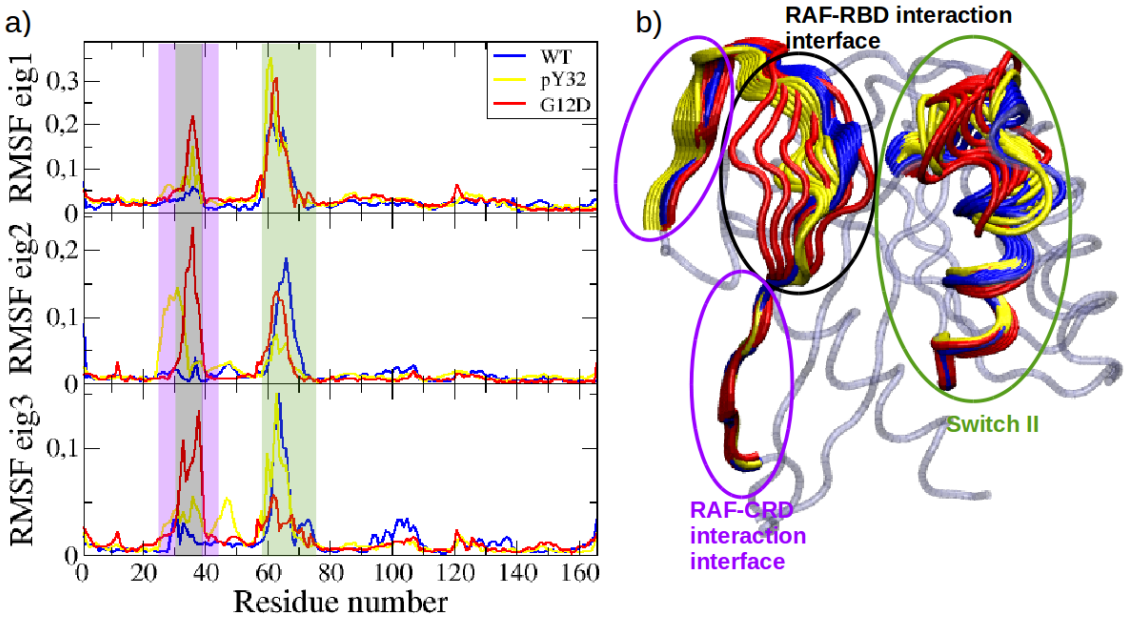

Figure 4.3: a) The comparison of the fluctuation profiles pertaining to the H-RAS systems along the first three eigenvectors. **b)** The obtained extreme structures along the first eigenvector are illustrated for H-RAS^{WT}, H-RAS^{pY32}, and H-RAS^{G12D} which are sequentially colored with blue, yellow, and red. The thickness of ribbons reflects the contributions of residues to overall dynamics.

Apart from the H-RAS isoform, the principal components of the K-RAS4B systems showed that the overall effect of tyrosyl phosphorylation was dominantly observed in the Switch II region and the corresponding region to the RAF-RBD interaction (See **Figure 4.4a** & **4.4b**). Yet, as opposed to the mutant H-RAS, the impact of the same mutant in the K-RAS4B isoform did not remarkably alter the global dynamic properties of the RAF-RBD interaction interface (See **Figure 4.4a**). More significantly, upon the phosphorylation, RAF-RBD interaction interface, which harbors Y32 as a residue having a relatively higher contribution to the overall dynamic properties, dominated the global dynamics, which might cause a distortion in the K-RAS4B-RAF-RBD interaction interface [129]. The projection of the trajectories pertaining to the K-RAS4B systems was also elucidated that the phosphorylation was more prone to drive conformational and dynamic changes in the Switch II region more than G12D mutation.

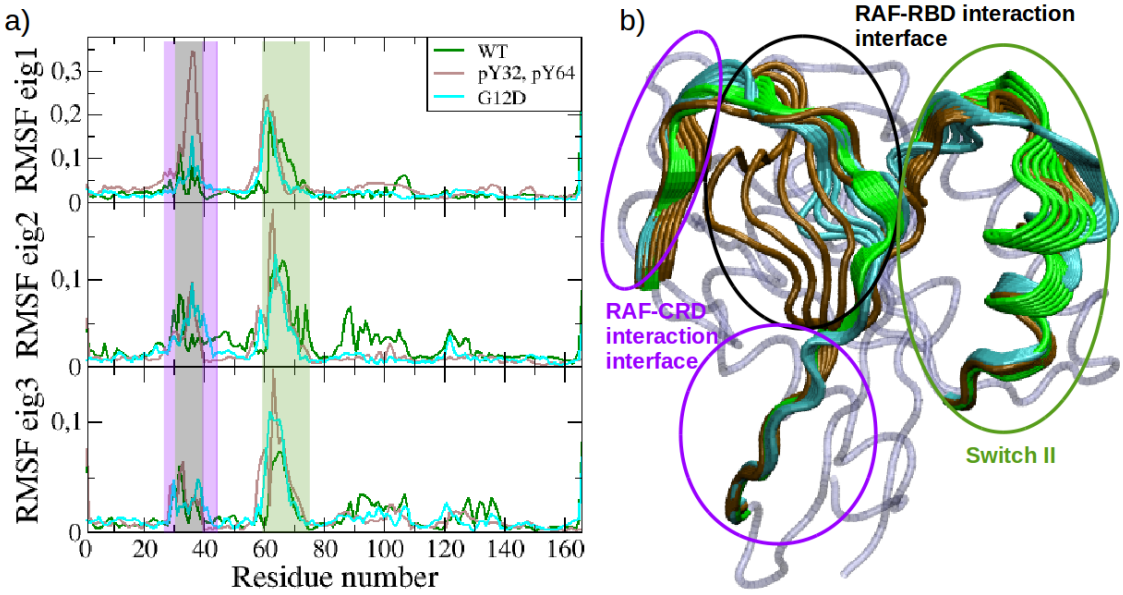

Figure 4.4: a) The comparison of the fluctuation profiles pertaining to the H-RAS systems along the first three eigenvectors. **b)** The obtained extreme structures along the first eigenvector are demonstrated for K-RAS4B^{WT}, K-RAS4B$^{pY32,\ pY64}$, and K-RAS4B^{G12D} which are, in seriatim, colored with green, brown, and cyan. The thickness of ribbons is directly proportional to the contributions of residues to overall dynamics.

In conclusion, in the case of tyrosyl phosphorylation and G12D mutation, the overall dynamics of the studied isoforms was dominated by the contribution of Switch I, which almost cover the RAF-RBD and -CRD interaction interface, and Switch II as it was consistent with local dynamic observations. Considering the importance of Switch, I for the effector-RAS interaction as well as its dominance on the overall dynamic properties,

this region seems to be a promising target site for altering the overall properties of the mutant systems.

4.4. Clustering Conformations Sampled in H-RAS^{G12D} and K-RAS4B^{G12D} and Identification of Possible Binding Sites on the Surface of the Most Probable Conformation of the Mutant Proteins

The sampled conformations throughout the trajectories of H-RAS^{G12D} and K-RAS4B^{G12D} were clustered based on the corroborated reaction coordinates which were the (i) distance between the side-chain oxygen of Thr35 and Pβ of GTP, (ii) backbone amide of Gly60 and Pβ of GTP, and (iii) side-chain oxygen of Gln61 and Pβ of GTP [107], [188], [189]. Consequently, the clustering showed that both K-RAS4B^{G12D} and H-RAS^{G12D} could adopt distinct states over the course of MD (See **Figure 4.5** & **4.6**). Subsequently, a frame, which represents the state 1 of each reaction coordinate that is the most probable state, was selected from the obtained trajectories of H-RAS^{G12D} and K-RAS4B^{G12D}.

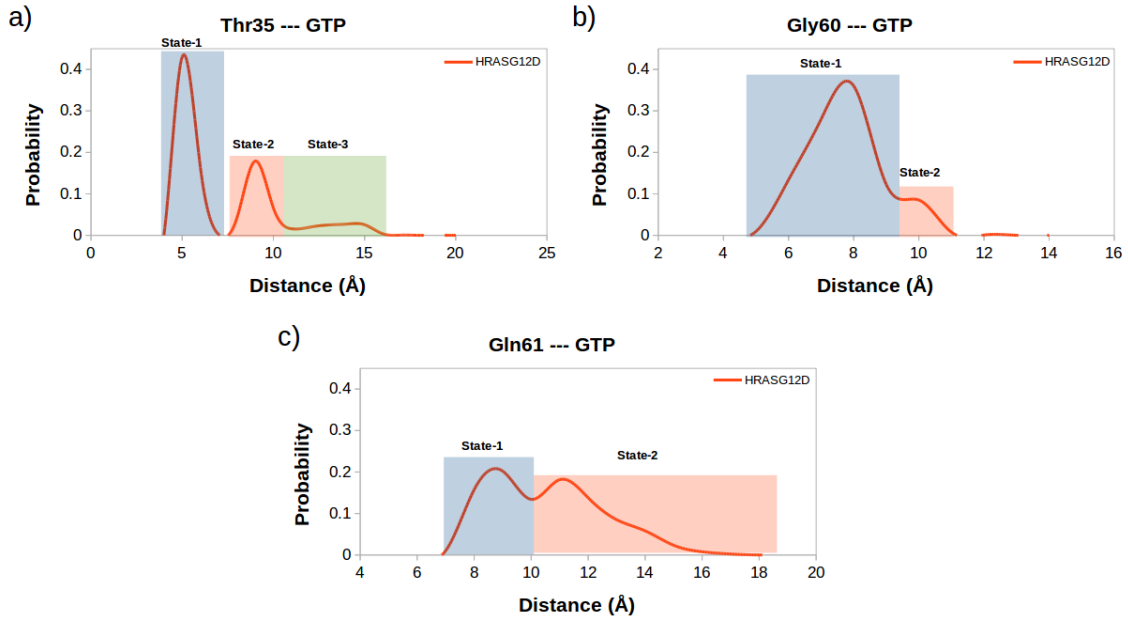

Figure 4.5: The probability distribution of the distance measured between the **a)** side-chain oxygen of Thr35 and Pβ of GTP, **b)** backbone amide of Gly60 and Pβ of GTP, and C. side-chain oxygen of Gln61 and Pβ of GTP throughout the obtained trajectories of H-RAS^{G12D}.

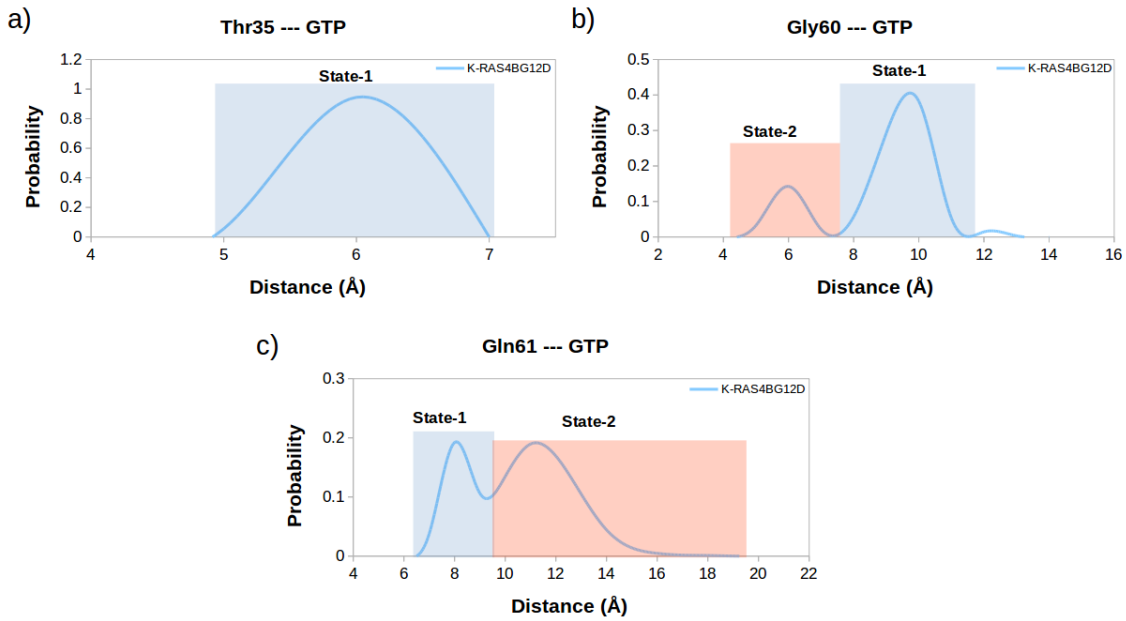

Figure 4.6: The probability distribution of the distance between the **a)** side-chain oxygen of Thr35 and Pβ of GTP, **b)** backbone amide of Gly60 and Pβ of GTP, and C. side-chain oxygen of Gln61 and Pβ of GTP throughout the obtained trajectories of K-RAS4B^{G12D}.

In light of the clustering, the selected frames, which correspond to the most probable states of the mutant systems, guided to determine possible binding cavities that are more likely to be accessible for drug molecules. As a result, both frames, which reflect the most probable ensemble of the mutant systems, are plausible to be targeted with small molecules towards the residues 29-34 that are accommodated on the Switch I region, as evidenced by relatively higher SiteScores (See **Table 4.1** and **4.2**).

Table 4.1: The SiteMap scores pertaining to most probable conformations sampled in the H-RAS^{G12D} trajectory.

SiteScore	Size	DScore	Volume	Exposure	Enclosure	Phob	Phil
1.03	194	0.92	466.14	0.48	0.74	0.26	1.43
0.70	25	0.67	81.29	0.63	0.69	1.47	0.66
0.66	22	0.63	101.87	0.78	0.64	0.96	0.60
0.54	20	0.38	68.60	0.77	0.61	0.00	1.23

Table 4.2: The SiteMap scores pertaining to most probable conformations sampled in the K-RAS4B^{G12D} trajectory.

SiteScore	Size	DScore	Volume	Exposure	Enclosure	Phob	Phil
1.01	231	0.96	503.18	0.55	0.71	0.45	1.25
0.60	32	0.55	67.57	0.73	0.53	0.16	0.92
0.56	26	0.38	39.44	0.61	0.57	0.00	1.36

To sum up the importance of the SiteMap findings, since competitive binding of inhibitors does not seem possible due to high affinity of the endogenous ligands of RAS [9]–[11], [102], the above-mentioned possible target site may offer an alternative for the development of therapeutics. More importantly, it is also a part of Switch I, which builds up effector interaction site and harbors Tyr32 that regulates, in particular, RAF binding and intrinsic GTPase activity [14], [15], [52].

4.5. Pharmacophore Modeling of the Possible Pockets Identified on the Surfaces of the Mutant Systems and Searching for Small Molecules in the Databases

With an inference to the existence of a common possible binding cavity on the surfaces of both H-RAS^{G12D} and K-RAS4B^{G12D}, the pharmacophore features of the possible target site were determined by taking the orientation and chemical properties of the building block residues into consideration. To do so, the pharmacophore groups of the residues 29-34 were modeled (See **Figure 4.7a** and **4.7c**). Despite the fact that these residues are well-conserved residues among the isoforms [52], the orientational distinctions brought some differences in the pharmacophore models (Compare **Figure 4.7b** and **4.7d**). Subsequently, molecules having at least 3 pharmacophore matches with the pharmacophore features of the isoforms and a molecular weight of less than 550 kDa were retrieved from ZINC15 [164]–[166], DrugBank [175]–[178], DrugCentral [167]–[169], BindingDB [171], [172], [174], [190], CHEMBL [191], [192], and NCGC [170] databases. In the end, a total of 14,053 downloaded molecules from the databases fulfilled the criteria and docked to the apo form of H-RAS^{G12D}. In the same manner, a total of 132,425 molecules were docked to the apo form of K-RAS4B^{G12D}.

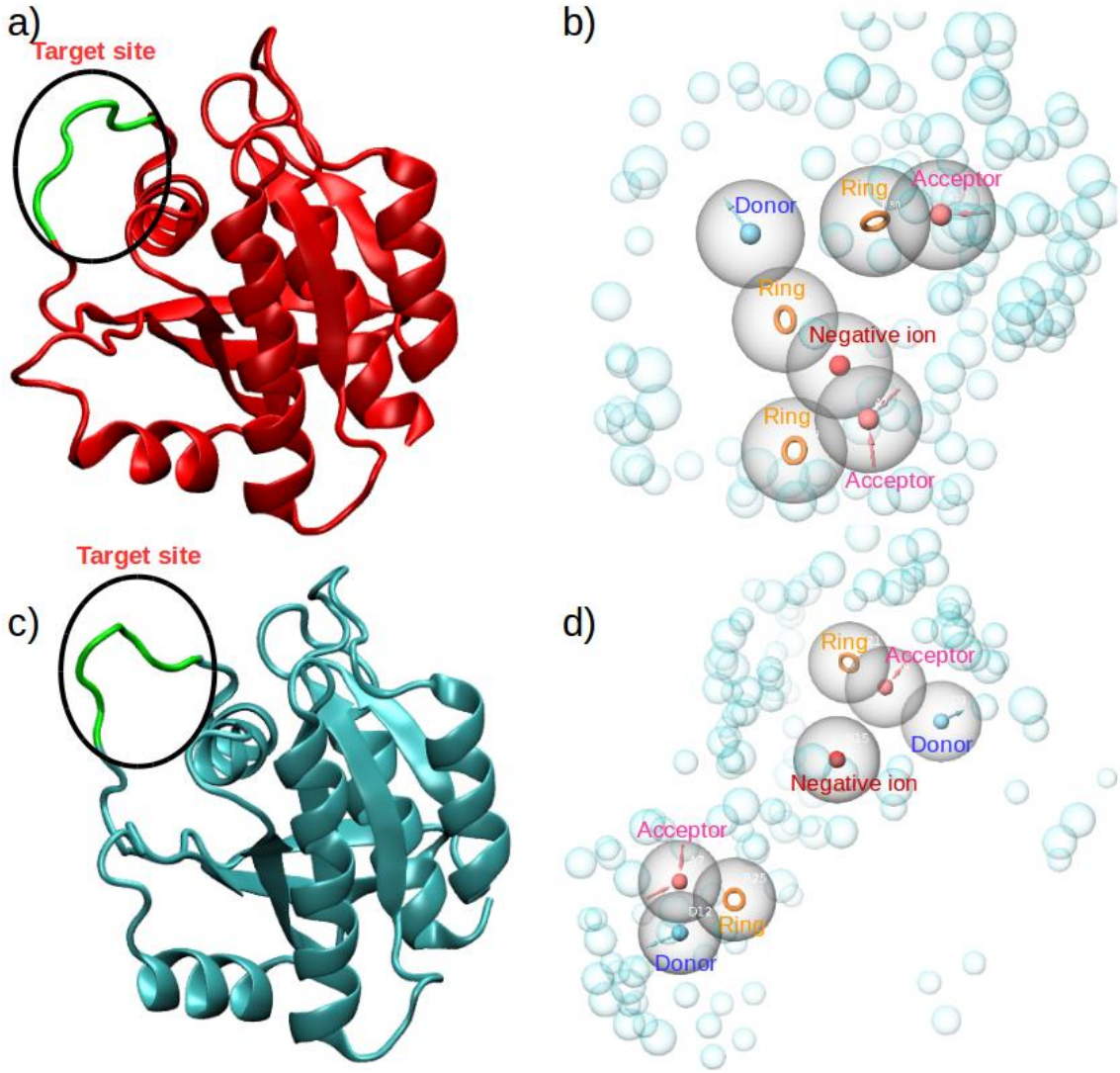

Figure 4.7: a) The identified target site on the surface of H-RAS^{G12D}. **b)** The modeled pharmacophore features of the residues 29-34, which constitutes the target site. **c)** The discerned target site on the surface of K-RAS4B^{G12D}. **d)** The modeled pharmacophore groups of the residues 29-34, which forms the target site.

The obtained ligand-H-RAS^{G12D} and -K-RAS4B^{G12D} complexes were assessed according to GScores as well as the orientation of the molecules with respect to the nucleotide-binding pocket. With this in mind, the comparison of GScores showed that molecules having a similar topology to GTP were more likely to be docked to the apo-form of the protein with a lower GScore (Compare **Figure 4.8a**/**4.9a** and **4.8b**/**4.9b**). Nevertheless, such molecules were not found to be promising since they were placed within the nucleotide-binding pocket, which is not physiologically plausible due to the high affinity of GTP/GDP molecules [9]–[11], [102]. For this reason, molecules that were orthogonal to the nucleotide-binding pocket were evaluated as promising candidates to be tested by MD simulations (See **Figure 4.8b** & **4.9b**).

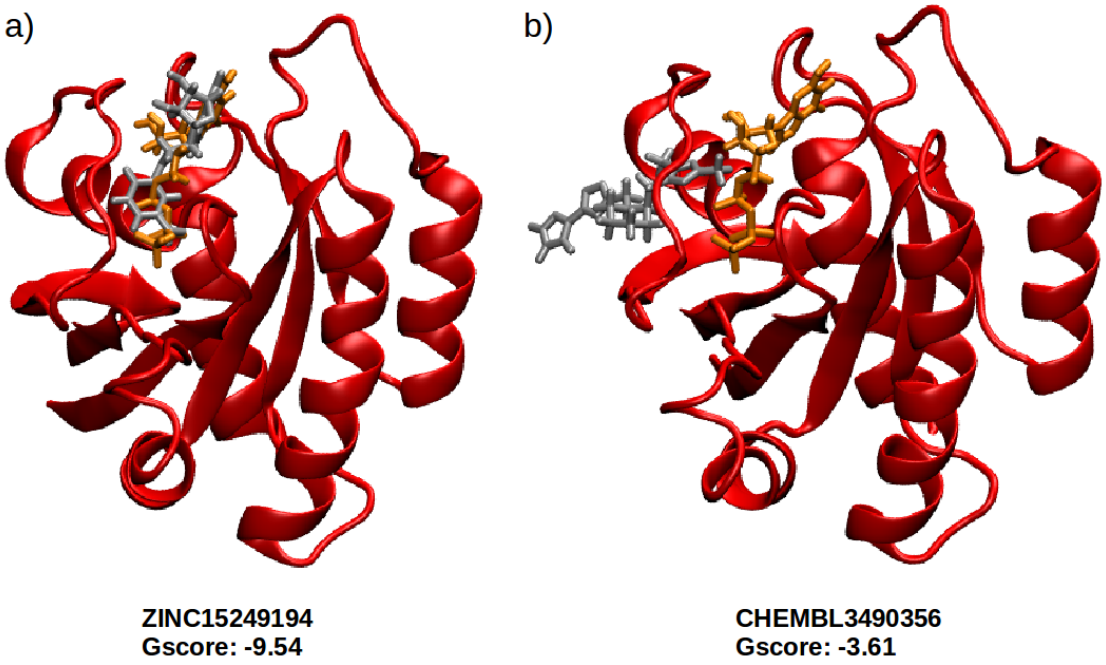

Figure 4.8: a) An example of unsuccessfully binding pose for H-RAS^{G12D}. **b)** An example of the binding pose that interferes with GTP. The GTP molecule is colored orange and ligands are shown in silver.

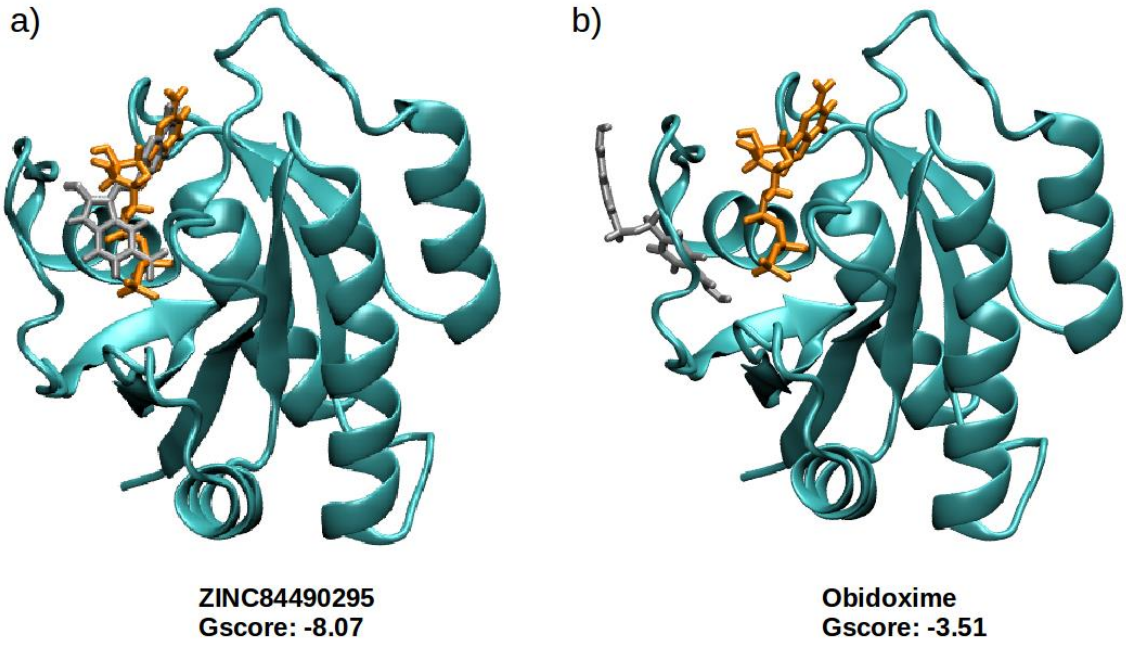

Figure 4.9: a) An example of unsuccessfully binding pose for K-RAS4B^{G12D}. **b)** An example of the binding pose that interferes with GTP. The GTP molecule is colored orange and ligands are shown in silver.

4.6. MD Simulations Revealed Molecules That Could Trigger Dynamic and Structural Alterations in the Mutant Systems Which Are Similar to Those Seen in the Phosphorylated Counterparts

With the aim of identifying molecules that could trigger similar dynamic and structural features to those of the phosphorylated systems, the impact of the ligands on the structural properties of the G12D mutant systems was explored and comprehensively compared with alterations driven by the tyrosyl phosphorylation. To this end, the selected molecules having a perpendicular orientation to the nucleotide-binding pocket of H-RAS^{G12D}/K-RAS4B^{G12D} were simulated in complex with their corresponding ligands (See **Table 4.3**). Subsequently, the ligand-H-RAS^{G12D} complexes were evaluated over the course of MD based on (i) the distance measured between the side-chain oxygen of Tyr32 and Pβ atom as well as the exposure of Tyr32, (ii) the relative change in the RMSF of Tyr32, (iii) the average difference in the RMSF of RAF-RBD and RAF-CRD interaction interfaces with respect to the H-RAS^{G12D} system. Having said that, the ligand-K-RAS4B^{G12D} complexes were investigated by devoting attention to (i) the distance measured between the side-chain oxygen and Pβ atom together with exposure of Tyr32, (ii) the relative change in the RMSF of Tyr32, and (iii) the mean of change in the RMSF of RAF-RBD interaction interface with respect to the K-RAS4B^{G12D} system. Finally, ligands that are bound to H-RAS^{G12D} are classified as promising if they increase the distance measured between the mention atom pairs as well as make Tyr32 exposed. With these in mind, it is also anticipated to increase the mobility of RAF-RBD and RAF-CRD domains. In parallel to these criteria, promising ligands that are bound to K-RAS4B^{G12D} are expected to raise the same distance between the atom pairs and make Tyr32 exposed like the phosphorylated system. Last but not least, a considerable elevation in the RMSF value of Tyr32 and RAF-RBD interface is another contributing factor to success criteria.

Table 4.3: GScores of the ligands used in MD simulations and corresponding simulation length.

Target	Molecule	GScore	MD time length (ns)
H-RAS^{G12D}	Cerubidine	-6.09	1776
H-RAS^{G12D}	ZINC16382913	-5.63	2880
H-RAS^{G12D}	Epirubicin	-5.44	2736
H-RAS^{G12D}	Imidafenacinum	-4.9	2608
H-RAS^{G12D}	Tranilast	-4.66	3078
H-RAS^{G12D}	Nilotinib	-4.61	1776
H-RAS^{G12D}	Paroxetine	-4.14	1066
H-RAS^{G12D}	ZINC16956714	-3.72	1728
H-RAS^{G12D}	CHEMBL3490356	-3.61	1977
H-RAS^{G12D}	ZINC08648721	-3.1	2880
K-RAS4B^{G12D}	ZINC07890675	-6.34	2880
K-RAS4B^{G12D}	ZINC94263682	-6.16	2112
K-RAS4B^{G12D}	ZINC72473488	-5.97	1920
K-RAS4B^{G12D}	ZINC91304948	-5.76	1920
K-RAS4B^{G12D}	Olodaterol	-5.41	1920
K-RAS4B^{G12D}	ZINC91562840	-4.75	1920
K-RAS4B^{G12D}	Glyconiazide	-4.64	2431
K-RAS4B^{G12D}	Cilastazol	-3.58	2547
K-RAS4B^{G12D}	Obidoxime	-3.51	2988
K-RAS4B^{G12D}	Perospirone	-3.39	1971

In light of the above-mentioned dynamics and structural alterations that are driven by tyrosyl phosphorylation, 10 of the ligands, which were bound to H-RAS^{G12D}, were thought of promising. First, like the H-RAS^{pY32} system, the treated H-RAS^{G12D} systems with ligands sampled longer distances of the predefined reaction coordinate, which, in turn, led to a distortion in the RAF interaction interface and facilitated the exposure of Tyr32. This suggests that the accessibility of GTP to nucleophilic water attacks might be potentiated, which might result in an increase in the intrinsic GTPase activity. As a closer look into each ligand, cerubidine, tranilast, nilotinib, ZINC16956714, CHEMBL3490356, and paroxetine were more prone to sample longer distances among the ligands studied, where Tyr32 of these systems were more likely to be found in the exposed state. (See **Figure 4.10a**, **4.10c**, **4.10d**, **4.10e**, **4.10f**, and **4.10j**). Nevertheless,

other ligands, namely ZINC16382913, ZINC08648721, imidafenacinum, and epirubicin, could also ascend the interval of the sampled distances with slightly lower probability, where Tyr32 became exposed throughout the trajectories (See **Figure 4.10b, 4.10g**, **4.10h**, and **4.10i**). Moreover, except CHEMBL3490356, imidafenacinum, and paroxetine, the rest of the ligands introduced flexibility to the RAF-RBD interface as in line with the phosphorylated counterpart of H-RAS. Lastly, it is also crucial to point out that all the studied ligands could not significantly increase the flexibility of the RAF-CRD interface (See **Table 4.4**). In spite of the failure of CHEMBL3490356 and paroxetine in elevating the flexibility of the both RAF-RBD and -CRD interaction interfaces, the change in the orientation of Tyr32 might be adequate to take control over the hyperactive H-RAS^{G12D}-RAF interaction. Last but not least, it is also significant to emphasize that all the ligands could increase the flexibility of Tyr32 as elucidated for the H-RAS^{pY32}. To wrap up the results of RMSF profiles, paroxetine, CHEMBL3490356, and imidafenacinum could not drive elevate the flexibility of the RAF-RBD interface. All the ligands could not also significantly increase the flexibility of the RAF-CRD interaction interface, whilst all the ligands, except nilotinib, paroxetine, and CHEMBL3490356 substantially increased the flexibility of Tyr32, which might be sufficient to cease aberrant RAF binding.

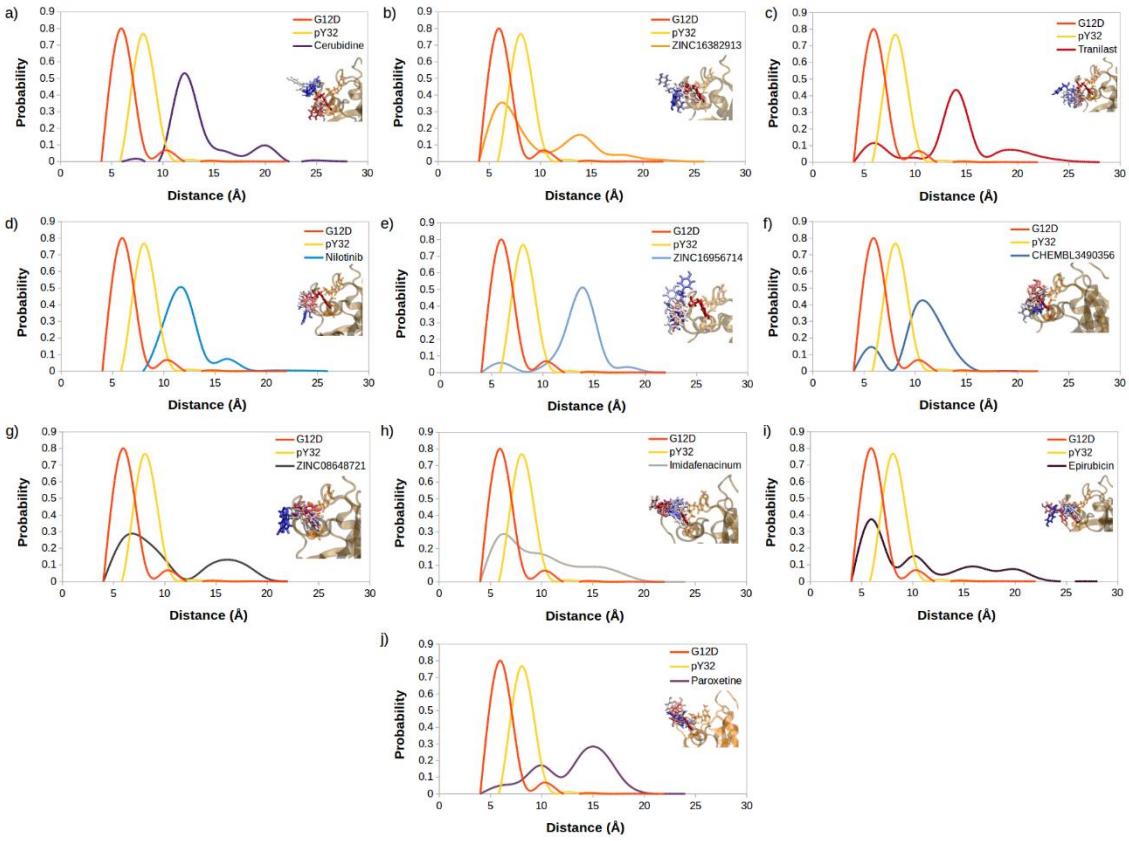

Figure 4.10: The probability distribution of the distance between the side-chain oxygen of Tyr32 and Pβ of GTP along with the conformation of Tyr32 in time-line during the obtained trajectories of **a)** cerubidine-, **b)** ZINC16382913-, **c)** tranilast-, **d)** nilotinib-, **e)** ZINC16956714-, **f)** CHEMBL3490356-, **g)** ZINC08648721-, **h)** imidafenacinum-, and **i)** epirubicin-, and **j)** paroxetine-bound H-RAS^{G12D}.

Table 4.4: The backbone RMSF difference of the residues that mediate RAF-RBD and RAF-CRD interaction in the ligand-H-RAS^{G12D} complexes.

System	**avg(ΔRMSF(RBD)) (nm)**	**avg(ΔRMSF(CRD)) (nm)**	**ΔRMSF(Tyr32) (nm)**
Cerubidine-H-RAS^{G12D}	0.14	0.01	0.25
ZINC16382913-H-RAS^{G12D}	0.12	0.05	0.10
Tranilast-H-RAS^{G12D}	0.16	0.05	0.22
Nilotinib-H-RAS^{G12D}	0.12	0.02	0.06
Paroxetine-H-RAS^{G12D}	-0.03	0.00	0.06
ZINC16956714-H-RAS^{G12D}	0.10	0.01	0.17
CHEMBL3490356-H-RAS^{G12D}	-0.01	0.00	0.05
ZINC08648721-H-RAS^{G12D}	0.20	0.02	0.29
Imidafenacinum-H-RAS^{G12D}	0.01	0.02	0.29
Epirubicin-H-RAS^{G12D}	0.19	0.05	0.30

In addition, 10 of ligand-K-RAS4B^{G12D} complexes were found to be promising in terms of shifting the dynamic and structural properties towards K-RAS4B$^{pY32,\ pY64}$. From top to bottom, it is important to keep in mind that the sampled distance between the Tyr32 and GTP ought to be higher than that of the K-RAS4B^{G12D} system so that Tyr32 might be accessible as discussed above. In parallel to this expectation, a recent study has shown that upon binding of RAF inhibitor to K-RAS4B^{G12D}, the distance between the side-chain oxygen of Tyr32 and GNP was shown to be enlarged [193]. From this perspective, all the reported ligands in **Table 4.5** distorted the RAF interaction interface and made Tyr32

exposed by increasing the distance measured between the mentioned atom pairs (See **Figure 4.11**). However, it is also paramount to indicate that ZINC91562840 could not obstacle the sampling of the distances that could not be sampled by the K-RAS4B$^{pY32,\ pY64}$ which might propagate K-RAS4B^{G12D}-RAF interaction in a controlled fashion (See **Figure 4.11c**). In this way, the ZINC91562840-bound K-RAS4B^{G12D} might gain its molecular switch, in which case it would not be forced to stay in the dark state [15]. More importantly, K-RAS4B$^{pY32,\ pY64}$ is known to be deprived of the intrinsic rate of GTPase activity, which might be presumably correlated to the propensity of Tyr32 to be found in the vicinity of the nucleotide-binding pocket. From this point of view, the dramatic change in the mentioned distance together with the alteration in the orientation of Tyr32 might also prompt the intrinsic rate of GTP hydrolysis by means of nucleophilic water attacks. Lastly, in line with the demystified structural and dynamic properties of K-RAS4B$^{pY32,\ pY64}$, the mobility of both RAF-RBD interaction interface and Tyr32 were significantly increased by the ligands as evidenced by the change in the RMSF values with respect to the K-RAS4B^{G12D} system (See **Table 4.5**).

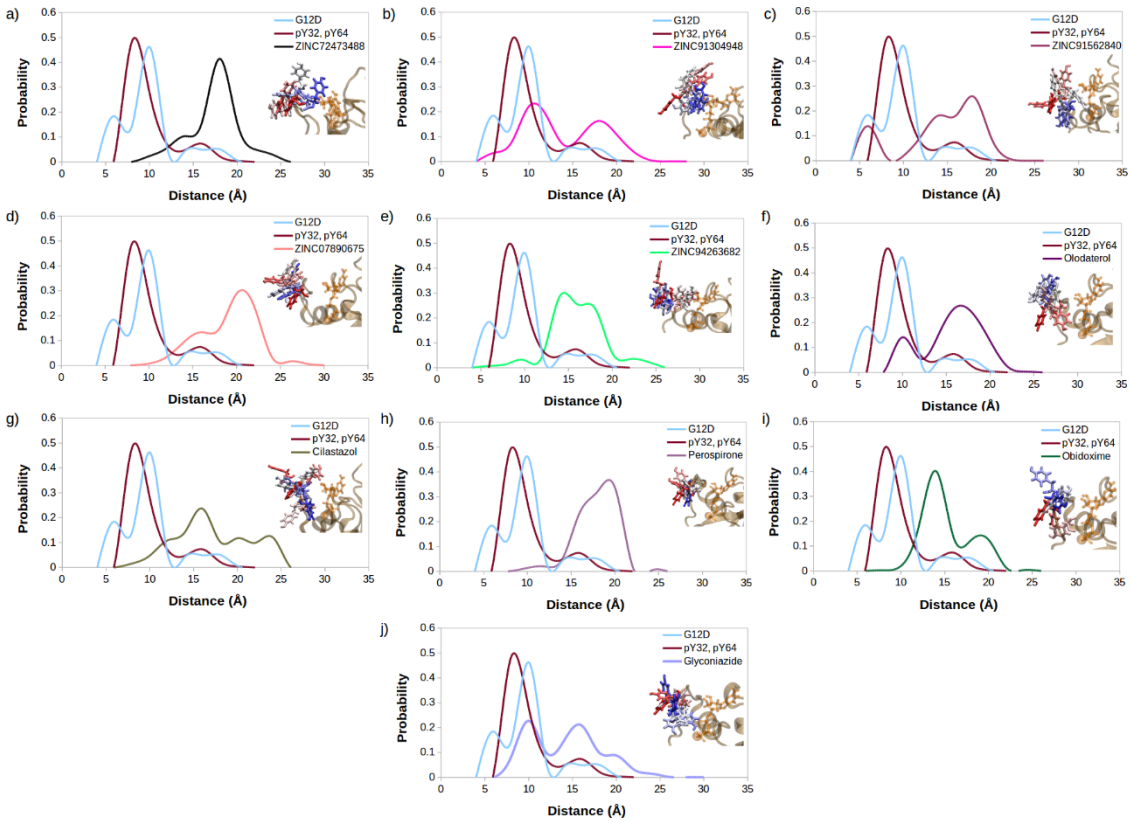

Figure 4.11: The probability distribution of the distance between the side-chain oxygen of Tyr32 and Pβ of GTP along with the conformation of Tyr32 in time-line during the obtained trajectories of **a)** ZINC72473488-, **b)** ZINC91304948-, **c)** ZINC91562840-, **d)** ZINC07890675-, **e)** ZINC94263682-, **f)** olodaterol-, **g)** cilastazol-, **h)** perospirone-, **i)** obidoxime, and **j)** glyconiazide-bound K-RAS^{G12D}.

Table 4.5: The backbone RMSF difference of the residues that mediate RAF-RBD in the ligand-K-RAS4B^{G12D}.

System	**avg(ΔRMSF(RBD)) (nm)**	**ΔRMSF(Tyr32) (nm)**
ZINC72473488-K-RAS4B^{G12D}	0.09	0.11
ZINC91304948-K-RAS4B^{G12D}	0.15	0.19
ZINC91562840-K-RAS4B^{G12D}	0.07	0.13
ZINC07890675-K-RAS4B^{G12D}	0.13	0.13
ZINC94263682-K-RAS4B^{G12D}	0.11	0.14
Olodaterol-K-RAS4B^{G12D}	0.09	0.10
Cilastazol-K-RAS4B^{G12D}	0.18	0.28
Perospirone-K-RAS4B^{G12D}	0.11	0.20
Obidoxime-K-RAS4B^{G12D}	0.17	0.18
Glyconiazide-K-RAS4B^{G12D}	0.12	0.17

4.7. The Conformations Sampled by RAS Mutants in Water and Membrane Are Different

RAS proteins are found in different cellular compartments such as cytoplasm, endoplasmic reticulum, Golgi apparatus, and cell membrane. Having a holistic

understanding of what kinds of conformations that RAS proteins can adopt in distinct cellular localization may pave the way for developing more selective drug molecules. With this regard, atomistic simulations of H-RAS^{G12D} and K-RAS4B^{G12D} were performed in the DMPC membrane model to elaborate on the effect of membrane on the reaction coordinates, which were utilized to cluster trajectories in the cytosolic state.

According to the obtained trajectories of the systems studied, the membrane restrained the sampled distances between the side-chain oxygen of Thr35 and Pβ of GTP as compared to the cytosolic state of the H-RAS^{G12D} system. Therefore, a tight coordination of the nucleotide-binding pocket by the Switch I region was more likely to be enforced (See **Figure 4.12a**). Despite the increased coordination of the nucleotide-binding pocket by Switch I, the membrane conversely caused to loss of the coordination of the nucleotide-binding pocket by the Switch II region (See **Figure 4.12b**). Consequently, considering structural studies, the membrane slightly shifted the dominant conformation from the inactive state 1 to 3, where the smaller distances between Thr35 and GTP could be sampled, and concurrently, the longer distances between Gly60 and GTP could be measured [107], [108], [188], [189]. Lastly, the measured distances between the side-chain oxygen of Gln61 and Pβ of GTP were also compared and shown that the membrane favored more the conformation that allows Gln61 to be found further away from the nucleotide-binding pocket (See **Figure 4.12c**). To sum up, the membrane induced dynamic distinctions in the reference atom-pairs distances that were utilized to cluster the trajectories. As such, upon binding to the membrane, the most frequently sampled conformation was different than the one selected for the cytosolic state of H-RAS^{G12D}.

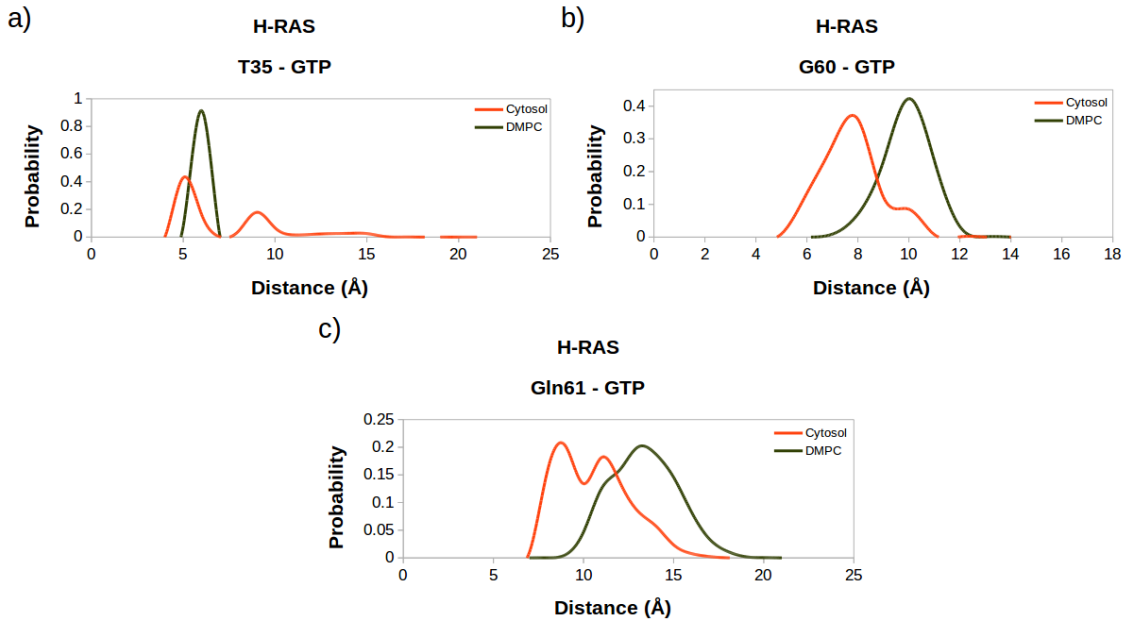

Figure 4.12: The probability distribution of the distance between the **a)** side-chain oxygen of Thr35 and Pβ of GTP, **b)** backbone amide of Gly60 and Pβ of GTP, and **c)** side-chain oxygen of Gln61 and Pβ of GTP over the course of the simulation pertaining to H-RAS^{G12D}.

Moreover, the DMPC membrane overall drove also some changes in the coordination of the nucleotide-binding pocket by the Switch II region of K-RAS4B^{G12D}, whilst the coordination of the pocket by the Switch I was retained almost the same over the time of the simulation (See Figure **4.13a** & **4.13b**). In detail, the membrane kept Gly60 in the vicinity of the nucleotide-binding pocket, thereby having tighter coordination of the pocket by Switch II as compared to the cytosolic state. In the light of the structural studies, the conformational state of the nucleotide-binding pocket predominantly tended to adopt state 1 in which the nucleotide-binding pocket is tightly coordinated by the Switch I and II regions [107], [108], [188], [189]. Lastly, the membrane increased the probability of sampling longer distances between the side-chain oxygen of Gln61 and Pβ of GTP (See **Figure 4.13c**). To sum up, despite the fact that the membrane did not cause alteration in the coordination of the nucleotide-binding pocket by the Switch I region, other sampled atom-pairs distances were different. This suggests that the most probable conformation that was selected from the trajectory of the cytosolic state of K-RAS4B^{G12D} was different than one that was predominantly sampled in the membrane.

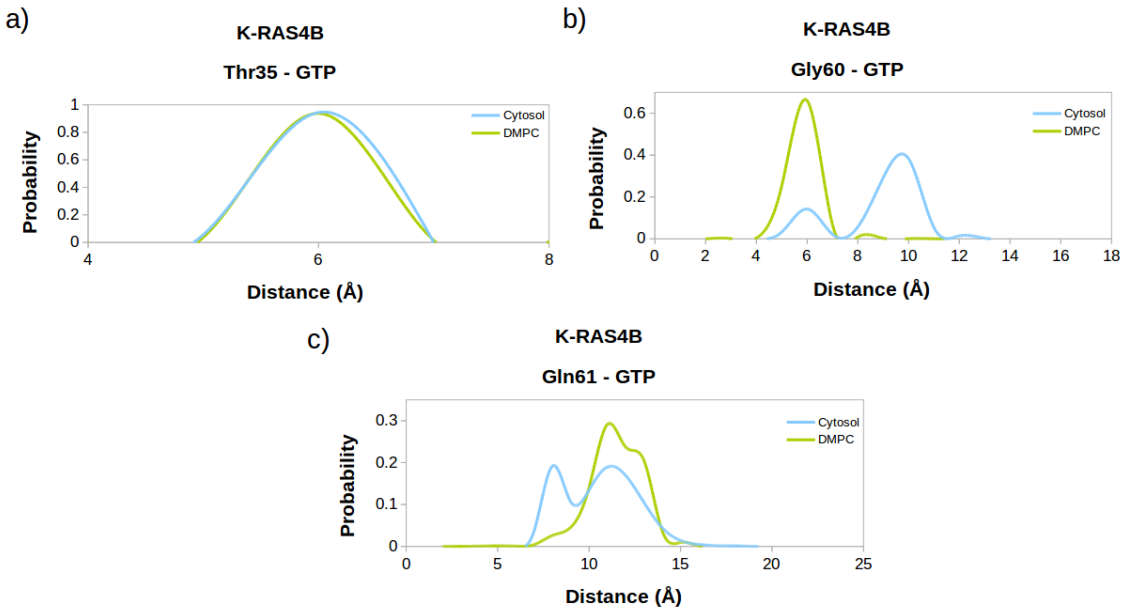

Figure 4.13: The probability distribution of the distance between the **a)** side-chain oxygen of Thr35 and Pβ of GTP, **b)** backbone amide of Gly60 and Pβ of GTP, and **c)** side-chain oxygen of Gln61 and Pβ of GTP throughout the obtained trajectories of K-RAS4B^{G12D}.

CHAPTER 5

5. CONCLUSIONS AND FUTURE WORK

Most of the RAS mutant proteins reduced the sensitivity of the protein to GAPs that also results in uncontrolled cellular signaling, thus known as the onset of tumorigenesis [4], [40]. In particular, the G12D mutant is one of the most prevalent ones that initiate several types of cancer among the studied isoforms [27], [41], [45]–[48]. In spite of the extraordinary studies that focus on the development of novel therapeutics that can bind to the RAS mutants, none of them have been admitted to be used in the clinic as RAS inhibitors. The lack of success is attributed to the absence of a deep pocket on the surface of the mutant proteins and the picomolar affinity of GTP/GDP to the nucleotide-binding pocket [9]–[11], [102]. On the other hand, concurrently, experimental studies have enlightened the effect of Src-kinase phosphorylation on RAS function. A recent study on H-RAS isoform has shown that phosphorylation of Tyr32 occludes RAF binding and increases the intrinsic rate of GTP hydrolysis [14]. In addition, a similar study on K-RAS4B isoform has indicated that even though the tyrosyl phosphorylation causes the disappearance of the intrinsic rate of GTP hydrolysis, it interrupts RAF binding [15]. From this point of view, we set out to have a holistic understanding of Src kinase-driven tyrosyl phosphorylation by employing MD simulations for GTP-bound H-RAS^{WT}, H-RAS^{G12D}, H-RAS^{pY32}, K-RAS4B^{WT}, K-RAS4B^{G12D}, and K-RAS4B$^{pY32,\ pY64}$. The comparison of the trajectories showed that both G12D mutation and tyrosyl phosphorylation of H-RAS caused an increase in the fluctuation of the RAF-RBD and -CRD interaction interfaces. The RAF-CRD interface of H-RAS^{pY32} and Tyr32 fluctuated the most among the studied H-RAS isoforms. Apart from the fluctuation profiles of the H-RAS systems, the mentioned mutation and phosphorylation of K-RAS4B increased the mobility of the RAF-RBD interaction interface and Ty32. As a side note, it is paramount to point out that the RAF-RBD interface of K-RAS4B$^{pY32,\ pY64}$ considerably fluctuated more than that of K-RAS4B^{G12D}. These changes, which were elucidated by simulations,

suggest that increasing the flexibility of Tyr32, the RAF-RBD and -CRD interfaces in H-RAS^{G12D} as well as Tyr32 and RAF-RBD in K-RAS4B^{G12D} may prevent mutant-RAF interaction. In addition to the comparison of RMSF profiles, the orientational dynamics of Tyr32 were scrutinized. Upon the phosphorylation of both isoforms, Tyr32 had more propensity to become exposed from the non-exposed state over the course of the simulations. This change in the orientation was shown by measuring the distance between Tyr32 and GTP for both isoforms, where exposure of this residue was correlated with longer sampled distances for the H-RAS isoform. On the other hand, K-RAS4B^{G12D} sampled relatively longer distances than K-RAS4B$^{pY32,\ pY64}$ although Tyr32 of K-RAS4B^{G12D} was not exposed. This might be concluded as the negatively charged phosphoryl group that was patched to Tyr32 is more likely to be repelled by negatively charged nearby residues, which might alter the orientation of Tyr32. This orientational change in K-RAS4B^{G12D} might presumably be possible in the case of sampling longer distances. This was indeed corroborated by glancing at the χ1 angle of the K-RAS4B systems, where K-RAS4B^{WT} and K-RAS4B$^{pY32,\ pY64}$ were tending to sample χ1 angles that allow Tyr32 to become exposed. As an advocator to local analysis, PCA showed that local structural and dynamical properties are in line with collective motion in the obtained trajectories of both H-RAS and K-RAS4B systems. In this way, it was assured that changing the dynamic properties of the Switch I region, which almost covers the RAF-RBD and -CRD interaction interface, would definitely induce some changes in the overall dynamics, thereby seems to be a good target site. Following the essential dynamic analysis, the obtained trajectories pertaining to H-RAS^{G12D} and K-RAS4B^{G12D} were clustered to discern the most probable conformation of the protein by exploiting the verified atom-pairs distances in the literature [107], [188], [189]. In light of the clustering, a binding pocket next to the nucleotide-binding pocket was identified and targeted with small molecules. Eventually, a total of 20 molecules were found as promising candidates because of their capability to resemble the dynamic and structural properties of phosphorylated counterparts in the mutant systems as revealed by MD simulations. As a side note, even though the proposed ligands for the mutant H-RAS were not capable of significantly increasing the fluctuation of the RAF-CRD interaction interface, the increase in the fluctuation of the RAF-RBD domain as well as exposure of Tyr32 might be sufficient to prevent RAF binding. Furthermore, as opposed to the tyrosyl phosphorylation of K-RAS4B, the repurposed molecules for K-RAS4B^{G12D}might also increase the intrinsic rate of GTP hydrolysis by increasing the accessibility of

nucleophilic water attacks to the GTP. More importantly, the ligands could increase the sampled distance between side-chain oxygen of Tyr32 and Pβ of GTP in K-RAS4B^{G12D} as shown in a recent experimental study, which suggests a potent K-RAS4B^{G12D} inhibitor for preventing RAF binding [193]. Notably, this ensemble-based virtual screening was conducted for the cytosolic state of the isoforms. On the other hand, it is known that RAS proteins are found in different cellular compartments. Therefore, the mutant systems were studied in a DMPC membrane model that is one of the most relevant compartments to active RAS proteins. The comparison of the atom pairs that were used for clustering the cytosolic mutant proteins illuminated that the membrane could allow mutant RAS proteins to sample a different prevalent conformation than those of the cytosolic states. Hence, as a future study, the structural and dynamic properties of the RAS proteins ought to be carefully compared to find the most probable ensemble of the mutant protein in each cellular compartment to pave the way for designing more selective and effective therapeutics.

BIBLIOGRAPHY

[1] R. L. Siegel, K. D. Miller, H. E. Fuchs, and A. Jemal, "Cancer Statistics, 2021," *CA: A Cancer Journal for Clinicians*, 2021, doi: 10.3322/caac.21654.

[2] I. A. Prior, P. D. Lewis, and C. Mattos, "A comprehensive survey of ras mutations in cancer," *Cancer Research*. 2012. doi: 10.1158/0008-5472.CAN-11-2612.

[3] I. A. Prior, F. E. Hood, and J. L. Hartley, "The frequency of Ras mutations in cancer," *Cancer Research*, p. canres.3682.2019, 2020, doi: 10.1158/0008-5472.can-19-3682.

[4] T. E. Mattox, X. Chen, Y. Y. Maxuitenko, A. B. Keeton, and G. A. Piazza, "Exploiting RAS nucleotide cycling as a strategy for drugging RAS-driven cancers," *International Journal of Molecular Sciences*. 2020. doi: 10.3390/ijms21010141.

[5] D. Vigil, J. Cherfils, K. L. Rossman, and C. J. Der, "Ras superfamily GEFs and GAPs: Validated and tractable targets for cancer therapy?," *Nature Reviews Cancer*. 2010. doi: 10.1038/nrc2960.

[6] A. D. Cox and C. J. Der, "Ras history: The saga continues," Small GTPases, 2010, doi: 10.4161/sgtp.1.1.12178.

[7] M. B. Myers, M. Banda, K. L. McKim, Y. Wang, M. J. Powell, and B. L. Parsons, "Breast Cancer Heterogeneity Examined by High-Sensitivity Quantification of PIK3CA, KRAS, HRAS, and BRAF Mutations in Normal Breast and Ductal Carcinomas," *Neoplasia (United States)*, vol. 18, no. 4, pp. 253–263, 2016, doi: 10.1016/j.neo.2016.03.002.

[8] J. H. Hah et al., "HRAS mutations and resistance to the epidermal growth factor receptor tyrosine kinase inhibitor erlotinib in head and neck squamous cell carcinoma cells," *Head and Neck*, 2014, doi: 10.1002/hed.23499.

[9] S. Gysin, M. Salt, A. Young, and F. McCormick, "Therapeutic strategies for targeting Ras proteins," *Genes and Cancer*, 2011, doi: 10.1177/1947601911412376.

[10] A. D. Cox, S. W. Fesik, A. C. Kimmelman, J. Luo, and C. J. Der, "Drugging the undruggable RAS: Mission Possible?," *Nature Reviews Drug Discovery*, vol. 13, no. 11, pp. 828–851, Nov. 2014, doi: 10.1038/nrd4389.

[11] L. G. Milroy and C. Ottmann, "The renaissance of Ras," *ACS Chemical Biology*. 2014. doi: 10.1021/cb500555h.

[12] D. Ni, X. Li, X. He, H. Zhang, J. Zhang, and S. Lu, "Drugging K-RasG12C through covalent inhibitors: Mission possible?," *Pharmacology and Therapeutics*. 2019. doi: 10.1016/j.pharmthera.2019.06.007.

[13] I. Khan, J. M. Rhett, and J. P. O'Bryan, "Therapeutic targeting of RAS: New hope for drugging the 'undruggable,'" *Biochimica et Biophysica Acta - Molecular Cell Research*. 2020. doi: 10.1016/j.bbamcr.2019.118570.

[14] S. Bunda et al., “Src promotes GTPase activity of Ras via tyrosine 32 phosphorylation,” *Proceedings of the National Academy of Sciences*, 2014, doi: 10.1073/pnas.1406559111.

[15] Y. Kano et al., “Tyrosyl phosphorylation of KRAS stalls GTPase cycle via alteration of switch I and II conformation,” *Nature Communications*, 2019, doi: 10.1038/s41467-018-08115-8.

[16] Y. Li et al., “Specific Substates of Ras to Interact with GAPs and Effectors: Revealed by Theoretical Simulations and FTIR Experiments,” *Journal of Physical Chemistry Letters*, vol. 9, no. 6, 2018, doi: 10.1021/acs.jpclett.8b00342.

[17] I. M. Ahearn, K. Haigis, D. Bar-Sagi, and M. R. Philips, “Regulating the regulator: Post-translational modification of RAS,” *Nature Reviews Molecular Cell Biology*. 2012. doi: 10.1038/nrm3255.

[18] J. J. Harvey, “An unidentified virus which causes the rapid production of tumours in mice [33],” *Nature*. 1964. doi: 10.1038/2041104b0.

[19] N. Tsuchida and S. Uesugi, “Structure and Functions of the Kirsten Murine Sarcoma Virus Genome: Molecular Cloning of Biologically Active Kirsten Murine Sarcoma Virus DNA,” *Journal of Virology*, 1981, doi: 10.1128/jvi.38.2.720-727.1981.

[20] N. Tsuchida, T. Ryder, and E. Ohtsubo, “Nucleotide sequence of the oncogene encoding the p21 transforming protein of Kirsten murine sarcoma virus,” *Science*, 1982, doi: 10.1126/science.6287573.

[21] E. H. Chang, M. A. Gonda, R. W. Ellis, E. M. Scolnick, and D. R. Lowy, “Human genome contains four genes homologous to transforming genes of Harvey and Kirsten murine sarcoma viruses,” *Proceedings of the National Academy of Sciences of the United States of America*, 1982, doi: 10.1073/pnas.79.16.4848.

[22] L. Wiesmüller and F. Wittinghofer, “Signal transduction pathways involving RAS,” *Cellular Signalling*, vol. 6, no. 3, pp. 247–267, Mar. 1994, doi: 10.1016/0898-6568(94)90030-2.

[23] P. Crespo and J. León, “Ras proteins in the control of the cell cycle and cell differentiation,” *Cellular and Molecular Life Sciences*. 2000. doi: 10.1007/PL00000645.

[24] M. Drosten et al., “Genetic analysis of Ras signalling pathways in cell proliferation, migration and survival,” *The EMBO Journal*, vol. 29, no. 6, pp. 1091–1104, 2010, doi: 10.1038/emboj.2010.7.

[25] Y. Pylayeva-Gupta, E. Grabocka, and D. Bar-Sagi, “RAS oncogenes: weaving a tumorigenic web,” *Nature Reviews Cancer*, vol. 11, no. 11, pp. 761–774, 2011, doi: 10.1038/nrc3106.

[26] K. L. Bryant, J. D. Mancias, A. C. Kimmelman, and C. J. Der, “KRAS: Feeding pancreatic cancer proliferation,” *Trends in Biochemical Sciences*, vol. 39, no. 2. pp. 91–100, 2014. doi: 10.1016/j.tibs.2013.12.004.

[27] S. Lu et al., “Ras Conformational Ensembles, Allostery, and Signaling,” *Chemical Reviews*, vol. 116, no. 11, pp. 6607–6665, Jun. 2016, doi: 10.1021/acs.chemrev.5b00542.

[28] M. Barbacid, “Ras Genes,” *Annual Review of Biochemistry*, 1987, doi: 10.1146/annurev.biochem.56.1.779.

[29] N. I. Marín-Ramos, S. Ortega-Gutiérrez, and M. L. López-Rodríguez, “Blocking Ras inhibition as an antitumor strategy*,” Seminars in Cancer Biology*. 2019. doi: 10.1016/j.semcancer.2018.01.017.

[30] S. G. Klochkov, M. E. Neganova, and Y. R. Aleksandrova, “Promising Molecular Targets for Design of Antitumor Drugs Based on Ras Protein Signaling Cascades,” *Russian Journal of Bioorganic Chemistry*. 2020. doi: 10.1134/S1068162020050118.

[31] M. F. Moran, P. Polakis, F. McCormick, T. Pawson, and C. Ellis, “Protein-tyrosine kinases regulate the phosphorylation, protein interactions, subcellular distribution, and activity of p21ras GTPase-activating protein*,” Molecular and Cellular Biology*, 1991, doi: 10.1128/mcb.11.4.1804.

[32] M. Geyer and A. Wittinghofer, “GEFs, GAPs, GDIs and effectors: Taking a closer (3D) look at the regulation of Ras-related GTP-binding proteins,” *Current Opinion in Structural Biology*, 1997, doi: 10.1016/S0959-440X(97)80147-9.

[33] S. R. Sprang, “G proteins, effecters and GAPs: Structure and mechanism,” *Current Opinion in Structural Biology*, 1997, doi: 10.1016/S0959-440X(97)80157-1.

[34] J. L. Bos, H. Rehmann, and A. Wittinghofer, “GEFs and GAPs: Critical Elements in the Control of Small G Proteins,” *Cell*. 2007. doi: 10.1016/j.cell.2007.05.018.

[35] J. Cherfils and M. Zeghouf, “Regulation of Small GTPases by GEFs, GAPs, and GDIs,” *Physiological Reviews*, 2013, doi: 10.1152/physrev.00003.2012.

[36] N. Mitin, K. L. Rossman, and C. J. Der, “Signaling interplay in ras superfamily function,” *Current Biology*. 2005. doi: 10.1016/j.cub.2005.07.010.

[37] N. Vasan, J. L. Boyer, and R. S. Herbst, “A RAS renaissance: Emerging targeted therapies for KRAS-mutated non-small cell lung cancer,” *Clinical Cancer Research*. 2014. doi: 10.1158/1078-0432.CCR-13-1762.

[38] W. H. Kirsten and L. A. Mayer, “Morphologic responses to a murine erythroblastosis virus,” *Journal of the National Cancer Institute*, 1967, doi: 10.1093/jnci/39.2.311.

[39] A. Wittinghofer, K. Scheffzek, and M. R. Ahmadian, “The interaction of Ras with GTPase-activating proteins,” *FEBS letters*, 1997. doi: 10.1016/S0014-5793(97)00321-9.

[40] D. Vigil, J. Cherfils, K. L. Rossman, and C. J. Der, “Ras superfamily GEFs and GAPs: Validated and tractable targets for cancer therapy?,” *Nature Reviews Cancer*. 2010. doi: 10.1038/nrc2960.

[41] I. A. Prior, P. D. Lewis, and C. Mattos, “A comprehensive survey of ras mutations in cancer,” *Cancer Research*. 2012. doi: 10.1158/0008-5472.CAN-11-2612.

[42] K. H. Lim, B. B. Ancrile, D. F. Kashatus, and C. M. Counter, “Tumour maintenance is mediated by eNOS,” *Nature*, 2008, doi: 10.1038/nature06778.

[43] C. Bentley et al., “A requirement for wild-type Ras isoforms in mutant KRas-driven signaling and transformation,” *Biochemical Journal*, 2013, doi: 10.1042/BJ20121578.

[44] E. J. Brock, K. Ji, J. J. Reiners, and R. R. Mattingly, “How to Target Activated Ras Proteins: Direct Inhibition vs. Induced Mislocalization,” *Mini-Reviews in Medicinal Chemistry*, 2015, doi: 10.2174/1389557515666151001154002.

[45] A. G. Stephen, D. Esposito, R. G. Bagni, and F. McCormick, “Dragging ras back in the ring,” *Cancer Cell*. 2014. doi: 10.1016/j.ccr.2014.02.017.

[46] S. A. Forbes et al., “COSMIC: Exploring the world’s knowledge of somatic mutations in human cancer,” *Nucleic Acids Research*, 2015, doi: 10.1093/nar/gku1075.

[47] S. M. Sweeney et al., “AACR project genie: Powering precision medicine through an international consortium,” *Cancer Discovery*, 2017, doi: 10.1158/2159-8290.CD-17-0151.

[48] S. Vatansever, B. Erman, and Z. H. Gümüş, “Oncogenic G12D mutation alters local conformations and dynamics of K-Ras,” *Scientific Reports*, 2019, doi: 10.1038/s41598-019-48029-z.

[49] C. A. Ellis and G. Clark, “The importance of being K-Ras,” *Cellular Signalling*. 2000. doi: 10.1016/S0898-6568(00)00084-X.

[50] M. Quinlan and J. Settleman, “Isoform-specific ras functions in development and cancer,” *Future Oncology*. 2009. doi: 10.2217/14796694.5.1.105.

[51] E. Castellano and E. Santos, “Functional specificity of Ras isoforms: So similar but so different,” *Genes and Cancer*, 2011, doi: 10.1177/1947601911408081.

[52] A. A. Gorfe, B. J. Grant, and J. A. McCammon, “Mapping the Nucleotide and Isoform-Dependent Structural and Dynamical Features of Ras Proteins,” *Structure*, 2008, doi: 10.1016/j.str.2008.03.009.

[53] G. Buhrman et al., “Analysis of binding site hot spots on the surface of Ras GTPase,” *Journal of Molecular Biology*, 2011, doi: 10.1016/j.jmb.2011.09.011.

[54] J. P. O’Bryan, “Pharmacological targeting of RAS: Recent success with direct inhibitors,” *Pharmacological Research*. 2019. doi: 10.1016/j.phrs.2018.10.021.

[55] I. Khan, J. M. Rhett, and J. P. O’Bryan, “Therapeutic targeting of RAS: New hope for drugging the ‘undruggable,’” *Biochimica et Biophysica Acta - Molecular Cell Research*, vol. 1867, no. 2, p. 118570, 2020, doi: 10.1016/j.bbamcr.2019.118570.

[56] M. Spoerner, A. Nuehs, P. Ganser, C. Hermann, A. Wittinghofer, and H. R. Kalbitzer, “Conformational states of ras complexed with the GTP analogue GppNHp or GppCH2p: Implications for the interaction with effector proteins,” *Biochemistry*, 2005, doi: 10.1021/bi0488000.

[57] M. Geyer, T. Schweins, C. Herrmann, T. Prisner, A. Wittinghofer, and H. R. Kalbitzer, “Conformational transitions in p21(ras) and in its complexes with the effector protein Raf-RBD and the GTPase activating protein GAP,” *Biochemistry*, 1996, doi: 10.1021/bi952858k.

[58] C. W. Johnson and C. Mattos, “The allosteric switch and conformational states in ras gtpase affected by small molecules,” *Enzymes*, 2013. doi: 10.1016/B978-0-12-416749-0.00003-8.

[59] S. M. Franken, A. Lautwein, M. Geyer, K. Scheffzek, H. R. Kalbitzer, and A. Wittinghofer, “Three-dimensional structures and properties of a transforming and a nontransforming glycine-12 mutant of p21H-ras,” *Biochemistry*, 1993.

[60] T. Maurer et al., “Small-molecule ligands bind to a distinct pocket in Ras and inhibit SOS-mediated nucleotide exchange activity,” *Proceedings of the National Academy of Sciences*, 2012, doi: 10.1073/pnas.1116510109.

[61] S. Muraoka et al., “Crystal structures of the state 1 conformations of the GTP-bound H-Ras protein and its oncogenic G12V and Q61L mutants,” *FEBS Letters*, 2012, doi: 10.1016/j.febslet.2012.04.058.

[62] J. M. Ostrem, U. Peters, M. L. Sos, J. A. Wells, and K. M. Shokat, “K-Ras(G12C) inhibitors allosterically control GTP affinity and effector interactions,” *Nature*, 2013, doi: 10.1038/nature12796.

[63] J. C. Hunter, A. Manandhar, M. A. Carrasco, D. Gurbani, S. Gondi, and K. D. Westover, “Biochemical and Structural Analysis of Common Cancer-Associated KRAS Mutations,” *Molecular Cancer Research*, 2015, doi: 10.1158/1541-7786.mcr-15-0203.

[64] S. Xu, B. N. Long, G. H. Boris, A. Chen, S. Ni, and M. A. Kennedy, “Structural insight into the rearrangement of the switch I region in GTP-bound G12A K-Ras,” *Acta Crystallographica Section D Structural Biology*, 2017, doi: 10.1107/s2059798317015418.

[65] M. Zeng et al., “Potent and Selective Covalent Quinazoline Inhibitors of KRAS G12C,” *Cell Chemical Biology*, 2017, doi: 10.1016/j.chembiol.2017.06.017.

[66] A. Sayyed-Ahmad, P. Prakash, and A. A. Gorfe, “Distinct dynamics and interaction patterns in H- and K-Ras oncogenic P-loop mutants,” *Proteins: Structure, Function and Bioinformatics*, 2017, doi: 10.1002/prot.25317.

[67] S. Vatansever, B. Erman, and Z. H. Gümüş, “Comparative effects of oncogenic mutations G12C, G12V, G13D, and Q61H on local conformations and dynamics of K-Ras,” *Computational and Structural Biotechnology Journal*, vol. 18, pp. 1000–1011, 2020, doi: 10.1016/j.csbj.2020.04.003.

[68] J. F. Hancock, H. Paterson, and C. J. Marshall, “A polybasic domain or palmitoylation is required in addition to the CAAX motif to localize p21ras to the plasma membrane,” *Cell*, 1990, doi: 10.1016/0092-8674(90)90294-O.

[69] E. Choy et al., “Endomembrane trafficking of ras: The CAAX motif targets proteins to the ER and Golgi,” *Cell*, 1999, doi: 10.1016/S0092-8674(00)80607-8.

[70] V. K. Chiu et al., “Ras signalling on the endoplasmic reticulum and the Golgi,” *Nature Cell Biology*, 2002, doi: 10.1038/ncb783.

[71] T. G. Bivona et al., “Phospholipase Cγ activates Ras on the Golgi apparatus by means of RasGRP1,” *Nature*, 2003, doi: 10.1038/nature01806.

[72] B. Casar et al., “Ras Subcellular Localization Defines Extracellular Signal-Regulated Kinase 1 and 2 Substrate Specificity through Distinct Utilization of Scaffold Proteins,” *Molecular and Cellular Biology*, 2009, doi: 10.1128/mcb.01359-08.

[73] I. M. Ahearn, K. Haigis, D. Bar-Sagi, and M. R. Philips, “Regulating the regulator: Post-translational modification of RAS,” *Nature Reviews Molecular Cell Biology*, vol. 13, no. 1, pp. 39–51, 2012, doi: 10.1038/nrm3255.

[74] L. Brunsveld, H. Waldmann, and D. Huster, “Membrane binding of lipidated Ras peptides and proteins - The structural point of view,” *Biochimica et Biophysica Acta - Biomembranes*. 2009. doi: 10.1016/j.bbamem.2008.08.006.

[75] F. D. Tsai et al., “K-Ras4A splice variant is widely expressed in cancer and uses a hybrid membrane-targeting motif*,” Proceedings of the National Academy of Sciences of the United States of America*, 2015, doi: 10.1073/pnas.1412811112.

[76] P. J. Casey, P. A. Solski, C. J. Der, and J. E. Buss, “p21ras is modified by a farnesyl isoprenoid,” *Proceedings of the National Academy of Sciences of the United States of America*, 1989, doi: 10.1073/pnas.86.21.8323.

[77] M. C. Seabra, Y. Reiss, P. J. Casey, M. S. Brown, and J. L. Goldstein, “Protein farnesyltransferase and geranylgeranyltransferase share a common α subunit,” *Cell*, 1991, doi: 10.1016/0092-8674(91)90460-G.

[78] T. Scott Reid, K. L. Terry, P. J. Casey, and L. S. Beese, “Crystallographic analysis of CaaX prenyltransferases complexed with substrates defines rules of protein substrate selectivity,” *Journal of Molecular Biology*, 2004, doi: 10.1016/j.jmb.2004.08.056.

[79] J. R. Silvius and F. l’Heureux, “Fluorimetric Evaluation of the Affinities of Isoprenylated Peptides for Lipid Bilayers,” *Biochemistry*, 1994, doi: 10.1021/bi00176a034.

[80] V. L. Boyartchuk, M. N. Ashby, and J. Rine, “Modulation of ras and a-factor function by carboxyl-terminal proteolysis,” *Science*, 1997, doi: 10.1126/science.275.5307.1796.

[81] Q. Dai et al., “Mammalian prenylcysteine carboxyl methyltransferase is in the endoplasmic reticulum,” *Journal of Biological Chemistry*, 1998, doi: 10.1074/jbc.273.24.15030.

[82] A. J. Laude and I. A. Prior, “Palmitoylation and localisation of RAS isoforms are modulated by the hypervariable linker domain,” *Journal of Cell Science*, 2008, doi: 10.1242/jcs.020107.

[83] A. Mor and M. R. Philips, “Compartmentalized Ras/MAPK signaling*,” Annual Review of Immunology*. 2006. doi: 10.1146/annurev.immunol.24.021605.090723.

[84] J. R. Silvius, P. Bhagatji, R. Leventis, and D. Terrone, “K-ras4B and prenylated proteins lacking ‘second signals’ associate dynamically with cellular membranes,” *Molecular Biology of the Cell*, 2006, doi: 10.1091/mbc.E05-05-0408.

[85] C. Mattos, “Ras: Structural details to guide direct targeting,” *Aging*. 2015. doi: 10.18632/aging.100754.

[86] M. B. Ryan, C. J. Der, A. Wang-Gillam, and A. D. Cox, “Targeting RAS-mutant Cancers: Is ERK the Key?,” *Trends in Cancer*. 2015. doi: 10.1016/j.trecan.2015.10.001.

[87] C. Sheridan, “Drug developers refocus efforts on RAS,” *Nature Biotechnology*. 2016. doi: 10.1038/nbt0316-217.

[88] B. Sautier, C. F. Nising, and L. Wortmann, “Latest Advances Towards Ras Inhibition: A Medicinal Chemistry Perspective,” *Angewandte Chemie - International Edition*. 2016. doi: 10.1002/anie.201608270.

[89] A. R. Moore, S. C. Rosenberg, F. McCormick, and S. Malek, “RAS-targeted therapies: is the undruggable drugged?,” *Nature Reviews Drug Discovery*. 2020. doi: 10.1038/s41573-020-0068-6.

[90] A. Flemming, “RAS mimetic revealed,” *Nature Reviews Drug Discovery*, 2016, doi: 10.1038/nrd.2016.108.

[91] A. Flemming, “Anticancer drugs: RAS mimetic revealed,” *Nature Reviews Drug Discovery*. 2016. doi: 10.1038/nrd.2016.108.

[92] S. Lu, H. Jang, S. Gu, J. Zhang, and R. Nussinov, “Drugging Ras GTPase: A comprehensive mechanistic and signaling structural view,” *Chemical Society Reviews*. 2016. doi: 10.1039/c5cs00911a.

[93] J. M. L. Ostrem and K. M. Shokat, “Direct small-molecule inhibitors of KRAS: From structural insights to mechanism-based design,” *Nature Reviews Drug Discovery*. 2016. doi: 10.1038/nrd.2016.139.

[94] M. B. Ryan and R. B. Corcoran, “Therapeutic strategies to target RAS-mutant cancers,” *Nature Reviews Clinical Oncology*. 2018. doi: 10.1038/s41571-018-0105-0.

[95] P. Liu, Y. Wang, and X. Li, “Targeting the untargetable KRAS in cancer therapy,” *Acta Pharmaceutica Sinica B*. 2019. doi: 10.1016/j.apsb.2019.03.002.

[96] S. Lu, Q. Shen, and J. Zhang, “Allosteric Methods and Their Applications: Facilitating the Discovery of Allosteric Drugs and the Investigation of Allosteric Mechanisms,” *Accounts of Chemical Research*, 2019, doi: 10.1021/acs.accounts.8b00570.

[97] A. Mullard, “Cracking KRAS,” *Nature reviews. Drug discovery*. 2019. doi: 10.1038/d41573-019-00195-5.

[98] R. Spencer-Smith and J. P. O’Bryan, “Direct inhibition of RAS: Quest for the Holy Grail?,” *Seminars in Cancer Biology*. 2019. doi: 10.1016/j.semcancer.2017.12.005.

[99] Y. Qiu et al., “Targeting RAS phosphorylation in cancer therapy: Mechanisms and modulators,” *Acta Pharmaceutica Sinica B.* 2021. doi: 10.1016/j.apsb.2021.02.014.

[100] J. Canon et al., “The clinical KRAS(G12C) inhibitor AMG 510 drives anti-tumour immunity,” *Nature*, 2019, doi: 10.1038/s41586-019-1694-1.

[101] M. J. Duffy and J. Crown, “Drugging ‘undruggable’ genes for cancer treatment: Are we making progress?,” *International Journal of Cancer*, vol. 148, no. 1, pp. 8–17, 2021, doi: 10.1002/ijc.33197.

[102] H. Ledford, “The Ras renaissance,” *Nature*, vol. 520, no. 7547, pp. 278–280, 2015, doi: 10.1038/520278a.

[103] B. Papke and C. J. Der, “Drugging RAS: Know the enemy,” *Science*. 2017. doi: 10.1126/science.aam7622.

[104] G. L. James, J. L. Goldstein, and M. S. Brown, “Polylysine and CVIM sequences of K-RasB dictate specificity of prenylation and confer resistance to benzodiazepine peptidomimetic in vitro,” *Journal of Biological Chemistry*, 1995, doi: 10.1074/jbc.270.11.6221.

[105] C. A. Rowell, J. J. Kowalczyk, M. D. Lewis, and A. M. Garcia, “Direct demonstration of geranylgeranylation and farnesylation of Ki-Ras in vivo,” *Journal of Biological Chemistry*, 1997, doi: 10.1074/jbc.272.22.14093.

[106] D. B. Whyte et al., “K- and N-Ras are geranylgeranylated in cells treated with farnesyl protein transferase inhibitors,” *Journal of Biological Chemistry*, 1997, doi: 10.1074/jbc.272.22.14459.

[107] S. Lu, H. Jang, R. Nussinov, and J. Zhang, “The Structural Basis of Oncogenic Mutations G12, G13 and Q61 in Small GTPase K-Ras4B,” *Scientific Reports*, vol. 6, no. February, pp. 1–15, 2016, doi: 10.1038/srep21949.

[108] M. Ilter and O. Sensoy, “Catalytically Competent Non-transforming H-RASG12P Mutant Provides Insight into Molecular Switch Function and GAP-independent GTPase Activity of RAS,” *Scientific Reports*, 2019, doi: 10.1038/s41598-019-47481-1.

[109] I. C. Rosnizeck et al., “Stabilizing a weak binding state for effectors in the human ras protein by cyclen complexes,” *Angewandte Chemie - International Edition*, 2010, doi: 10.1002/anie.200907002.

[110] J. M. Ostrem, U. Peters, M. L. Sos, J. A. Wells, and K. M. Shokat, “K-Ras(G12C) inhibitors allosterically control GTP affinity and effector interactions,” *Nature*, 2013, doi: 10.1038/nature12796.

[111] M. P. Patricelli et al., “Selective inhibition of oncogenic KRAS output with small molecules targeting the inactive state,” *Cancer Discovery*, 2016, doi: 10.1158/2159-8290.CD-15-1105.

[112] M. R. Janes et al., “Targeting KRAS Mutant Cancers with a Covalent G12C-Specific Inhibitor,” *Cell*, 2018, doi: 10.1016/j.cell.2018.01.006.

[113] R. Hansen et al., “The reactivity-driven biochemical mechanism of covalent KRASG12Cinhibitors.,” *Nat. Struct. Mol. Biol.*, 2018, doi: 10.2210/pdb6b0v/pdb.

[114] D. S. Hong et al., “ KRAS G12C Inhibition with Sotorasib in Advanced Solid Tumors ,” *New England Journal of Medicine*, 2020, doi: 10.1056/nejmoa1917239.

[115] B. A. Lanman et al., “Discovery of a Covalent Inhibitor of KRASG12C (AMG 510) for the Treatment of Solid Tumors,” *Journal of Medicinal Chemistry*, 2020, doi: 10.1021/acs.jmedchem.9b01180.

[116] F. Marks, Protein Phosphorylation, *John Wiley & Sons*. 2007. doi: 10.1002/9783527615032.

[117] T. Y. Shih, M. O. Weeks, H. A. Young, and E. M. Scolnick, “Identification of a sarcoma virus-coded phosphoprotein in nonproducer cells transformed by Kirsten or Harvey murine sarcoma virus,” *Virology*, 1979, doi: 10.1016/0042-6822(79)90173-9.

[118] A. Papageorge, D. Lowy, and E. M. Scolnick, “Comparative biochemical properties of p21 ras molecules coded for by viral and cellular ras genes.,” *Journal of Virology*, 1982, doi: 10.1128/jvi.44.2.509-519.1982.

[119] J. John, M. Frech, and A. Wittinghofer, “Biochemical properties of Ha-ras encoded p21 mutants and mechanism of the autophosphorylation reaction,” *Journal of Biological Chemistry*, 1988, doi: 10.1016/s0021-9258(18)37854-2.

[120] C. Washington et al., “A conserved, N-terminal tyrosine signal directs Ras for inhibition by Rabex-5,” *PLoS Genetics*, 2020, doi: 10.1371/journal.pgen.1008715.

[121] P. Y. Ting et al., “Tyrosine phosphorylation of RAS by ABL allosterically enhances effector binding,” *FASEB Journal*, 2015, doi: 10.1096/fj.15-271510.

[122] C. Yin et al., “Pharmacological Targeting of STK19 Inhibits Oncogenic NRAS-Driven Melanomagenesis,” *Cell*, 2019, doi: 10.1016/j.cell.2019.01.002.

[123] T. G. Bivona et al., “PKC regulates a farnesyl-electrostatic switch on K-Ras that promotes its association with Bcl-XL on mitochondria and induces apoptosis,” *Molecular Cell*, 2006, doi: 10.1016/j.molcel.2006.01.012.

[124] W. J. Jeong et al., “Ras stabilization through aberrant activation of Wnt/β-catenin signaling promotes intestinal tumorigenesis,” *Science Signaling*, 2012, doi: 10.1126/scisignal.2002242.

[125] Y. Wang et al., “Mechanistic insights into the effect of phosphorylation on Ras conformational dynamics and its interactions with cell signaling proteins,” *Computational and Structural Biotechnology Journal*, vol. 19, pp. 1184–1199, 2021, doi: 10.1016/j.csbj.2021.01.044.

[126] R. Roskoski, “Src protein-tyrosine kinase structure, mechanism, and small molecule inhibitors,” *Pharmacological Research*, 2015, doi: 10.1016/j.phrs.2015.01.003.

[127] S. Bunda et al., “Inhibition of SHP2-mediated dephosphorylation of Ras suppresses oncogenesis,” *Nature Communications*, 2015, doi: 10.1038/ncomms9859.

[128] H. Gohlke, C. Kiel, and D. A. Case, “Insights into protein-protein binding by binding free energy calculation and free energy decomposition for the Ras-Raf and Ras-RalGDS complexes.,” *Journal of molecular biology*, 2003, doi: 10.1016/S0022-2836(03)00610-7.

[129] S. K. Fetics et al., “Allosteric effects of the oncogenic rasq61l mutant on raf-RBD,” *Structure*, vol. 23, no. 3, pp. 505–516, 2015, doi: 10.1016/j.str.2014.12.017.

[130] Y. Wang et al., “Mechanistic insights into the effect of phosphorylation on Ras conformational dynamics and its interactions with cell signaling proteins,” *Computational and Structural Biotechnology Journal*, 2021, doi: 10.1016/j.csbj.2021.01.044.

[131] E. F. Pai, U. Krengel, G. A. Petsko, R. S. Goody, W. Kabsch, and A. Wittinghofer, “Refined crystal structure of the triphosphate conformation of H-ras p21 at 1.35 A resolution: implications for the mechanism of GTP hydrolysis.,” *EMBO J.*, vol. 9, pp. 2351–2359, 1990, doi: 10.2210/PDB5P21/PDB.

[132] S. M. Franken et al., “Three-Dimensional Structures and Properties of a Transforming and a Nontransforming Glycine-12 Mutant of p21H-ras,” *Biochemistry*, 1993, doi: 10.1021/bi00084a005.

[133] H. M. Berman et al., “The Protein Data Bank,” *Nucleic Acids Research*. 2000. doi: 10.1093/nar/28.1.235.

[134] S. K. Burley et al., “RCSB Protein Data Bank: powerful new tools for exploring 3D structures of biological macromolecules for basic and applied research and education in fundamental biology, biomedicine, biotechnology, bioengineering and energy sciences,” *Nucleic Acids Research*, 2021, doi: 10.1093/nar/gkaa1038.

[135] C. R. Søndergaard, M. H. M. Olsson, M. Rostkowski, and J. H. Jensen, “Improved Treatment of Ligands and Coupling Effects in Empirical Calculation and Rationalization of p K a Values,” *Journal of Chemical Theory and Computation*, vol. 7, no. 7, pp. 2284–2295, Jul. 2011, doi: 10.1021/ct200133y.

[136] M. H. M. Olsson, C. R. SØndergaard, M. Rostkowski, and J. H. Jensen, “PROPKA3: Consistent treatment of internal and surface residues in empirical p K a predictions,” *Journal of Chemical Theory and Computation*, 2011, doi: 10.1021/ct100578z.

[137] L. N. Johnson and R. J. Lewis, “Structural basis for control by phosphorylation,” *Chemical Reviews*. 2001. doi: 10.1021/cr000225s.

[138] P. Mark and L. Nilsson*, “Structure and Dynamics of the TIP3P, SPC, and SPC/E Water Models at 298 K,” *The Journal of Physical Chemistry A*, 2001, doi: 10.1021/JP003020W.

[139] J. C. Phillips et al., “Scalable molecular dynamics on CPU and GPU architectures with NAMD,” *Journal of Chemical Physics*, 2020, doi: 10.1063/5.0014475.

[140] K. Vanommeslaeghe et al., “CHARMM general force field: A force field for drug-like molecules compatible with the CHARMM all-atom additive biological force fields,” *Journal of Computational Chemistry*, 2010, doi: 10.1002/jcc.21367.

[141] R. B. Best et al., “Optimization of the Additive CHARMM All-Atom Protein Force Field Targeting Improved Sampling of the Backbone ϕ, ψ and Side-Chain

χ 1 and χ 2 Dihedral Angles," *Journal of Chemical Theory and Computation*, vol. 8, no. 9, pp. 3257–3273, Sep. 2012, doi: 10.1021/ct300400x.

[142] K. Vanommeslaeghe and A. D. MacKerell, "Automation of the CHARMM general force field (CGenFF) I: Bond perception and atom typing," *Journal of Chemical Information and Modeling*, 2012, doi: 10.1021/ci300363c.

[143] W. Yu, X. He, K. Vanommeslaeghe, and A. D. MacKerell, "Extension of the CHARMM general force field to sulfonyl-containing compounds and its utility in biomolecular simulations," *Journal of Computational Chemistry*, 2012, doi: 10.1002/jcc.23067.

[144] I. Soteras Gutiérrez et al., "Parametrization of halogen bonds in the CHARMM general force field: Improved treatment of ligand–protein interactions," *Bioorganic and Medicinal Chemistry*, 2016, doi: 10.1016/j.bmc.2016.06.034.

[145] U. Essmann, L. Perera, M. L. Berkowitz, T. Darden, H. Lee, and L. G. Pedersen, "A smooth particle mesh Ewald method," *The Journal of Chemical Physics*, 1995, doi: 10.1063/1.470117.

[146] I. Andricioaei and M. Karplus, "Particle mesh Ewald: An N·log(N) method for Ewald sums in large systems The," *Statistical Mechanics of Fluid Mixtures The Journal of Chemical Physics*, 2001.

[147] L. Tong, A. M. de Vos, M. V. Milburn, and S. H. Kim, "Crystal structures at 2.2 Å resolution of the catalytic domains of normal ras protein and an oncogenic mutant complexed with GDP," *Journal of Molecular Biology*, 1991, doi: 10.1016/0022-2836(91)90753-S.

[148] Schrödinger, "Schrödinger Release 2018-4: Maestro, Schrödinger, LLC," Maestro-Desmond Interoperability Tools, Desmond Molecular Dynamics System. 2018.

[149] S. Jo, T. Kim, V. G. Iyer, and W. Im, "CHARMM-GUI: A web-based graphical user interface for CHARMM," *Journal of Computational Chemistry*, 2008, doi: 10.1002/jcc.20945.

[150] B. R. Brooks et al., "CHARMM: The biomolecular simulation program," *Journal of Computational Chemistry*, 2009, doi: 10.1002/jcc.21287.

[151] J. Lee et al., "CHARMM-GUI Input Generator for NAMD, GROMACS, AMBER, OpenMM, and CHARMM/OpenMM Simulations Using the CHARMM36 Additive Force Field," *Journal of Chemical Theory and Computation*, 2016, doi: 10.1021/acs.jctc.5b00935.

[152] S. Jo, T. Kim, and W. Im, "Automated builder and database of protein/membrane complexes for molecular dynamics simulations," *PLoS ONE*, 2007, doi: 10.1371/journal.pone.0000880.

[153] S. Jo, J. B. Lim, J. B. Klauda, and W. Im, "CHARMM-GUI membrane builder for mixed bilayers and its application to yeast membranes," *Biophysical Journal*, 2009, doi: 10.1016/j.bpj.2009.04.013.

[154] E. L. Wu et al., "CHARMM-GUI membrane builder toward realistic biological membrane simulations," *Journal of Computational Chemistry*. 2014. doi: 10.1002/jcc.23702.

[155] J. Lee, M. Hitzenberger, M. Rieger, N. R. Kern, M. Zacharias, and W. Im, "CHARMM-GUI supports the Amber force fields," *Journal of Chemical Physics*, 2020, doi: 10.1063/5.0012280.

[156] M. P. Jacobson, R. A. Friesner, Z. Xiang, and B. Honig, "On the role of the crystal environment in determining protein side-chain conformations," *Journal of Molecular Biology*, 2002, doi: 10.1016/S0022-2836(02)00470-9.

[157] M. P. Jacobson et al., "A Hierarchical Approach to All-Atom Protein Loop Prediction," *Proteins: Structure, Function and Genetics*, 2004, doi: 10.1002/prot.10613.

[158] T. Halgren, "New method for fast and accurate binding-site identification and analysis," *Chemical Biology and Drug Design*, 2007, doi: 10.1111/j.1747-0285.2007.00483.x.

[159] T. A. Halgren, "Identifying and characterizing binding sites and assessing druggability," *Journal of Chemical Information and Modeling*, 2009, doi: 10.1021/ci800324m.

[160] G. Madhavi Sastry, M. Adzhigirey, T. Day, R. Annabhimoju, and W. Sherman, "Protein and ligand preparation: Parameters, protocols, and influence on virtual screening enrichments," *Journal of Computer-Aided Molecular Design*, 2013, doi: 10.1007/s10822-013-9644-8.

[161] K. Roos et al., "OPLS3e: Extending Force Field Coverage for Drug-Like Small Molecules," *Journal of Chemical Theory and Computation*, 2019, doi: 10.1021/acs.jctc.8b01026.

[162] K. Loving, N. K. Salam, and W. Sherman, "Energetic analysis of fragment docking and application to structure-based pharmacophore hypothesis generation," *Journal of Computer-Aided Molecular Design*, 2009, doi: 10.1007/s10822-009-9268-1.

[163] N. K. Salam, R. Nuti, and W. Sherman, "Novel method for generating structure-based pharmacophores using energetic analysis," *Journal of Chemical Information and Modeling*, 2009, doi: 10.1021/ci900212v.

[164] J. J. Irwin and B. K. Shoichet, "ZINC - A free database of commercially available compounds for virtual screening," *Journal of Chemical Information and Modeling*, 2005, doi: 10.1021/ci049714+.

[165] J. J. Irwin, T. Sterling, M. M. Mysinger, E. S. Bolstad, and R. G. Coleman, "ZINC: A free tool to discover chemistry for biology," *Journal of Chemical Information and Modeling*, vol. 52, no. 7. pp. 1757–1768, 2012. doi: 10.1021/ci3001277.

[166] T. Sterling and J. J. Irwin, "ZINC 15 - Ligand Discovery for Everyone," *Journal of Chemical Information and Modeling*, 2015, doi: 10.1021/acs.jcim.5b00559.

[167] O. Ursu et al., "DrugCentral: Online drug compendium," *Nucleic Acids Research*, 2017, doi: 10.1093/nar/gkw993.

[168] O. Ursu et al., "DrugCentral 2018: An update," *Nucleic Acids Research*, 2019, doi: 10.1093/nar/gky963.

[169] S. Avram et al., “DrugCentral 2021 supports drug discovery and repositioning,” *Nucleic Acids Research,* 2021, doi: 10.1093/nar/gkaa997.

[170] R. Huang et al., “The NCGC pharmaceutical collection: A comprehensive resource of clinically approved drugs enabling repurposing and chemical genomics,” *Science Translational Medicine*. 2011. doi: 10.1126/scitranslmed.3001862.

[171] X. Chen, Y. Lin, and M. K. Gilson, “The binding database: Overview and user’s guide,” *Biopolymers*. 2001. doi: 10.1002/1097-0282(2002)61:2<127::AID-BIP10076>3.0.CO;2-N.

[172] X. Chen, Y. Lin, M. Liu, and M. K. Gilson, “The binding database: Data management and interface design,” *Bioinformatics,* 2002, doi: 10.1093/bioinformatics/18.1.130.

[173] T. Liu, Y. Lin, X. Wen, R. N. Jorissen, and M. K. Gilson, “BindingDB: A web-accessible database of experimentally determined protein-ligand binding affinities,” *Nucleic Acids Research,* 2007, doi: 10.1093/nar/gkl999.

[174] M. K. Gilson, T. Liu, M. Baitaluk, G. Nicola, L. Hwang, and J. Chong, “BindingDB in 2015: A public database for medicinal chemistry, computational chemistry and systems pharmacology,” *Nucleic Acids Research,* 2016, doi: 10.1093/nar/gkv1072.

[175] D. S. Wishart et al., “DrugBank: A knowledgebase for drugs, drug actions and drug targets,” *Nucleic Acids Research,* 2008, doi: 10.1093/nar/gkm958.

[176] C. Knox et al., “DrugBank 3.0: A comprehensive resource for ‘Omics’ research on drugs,” *Nucleic Acids Research,* 2011, doi: 10.1093/nar/gkq1126.

[177] V. Law et al., “DrugBank 4.0: Shedding new light on drug metabolism,” *Nucleic Acids Research*, 2014, doi: 10.1093/nar/gkt1068.

[178] D. S. Wishart et al., “DrugBank 5.0: A major update to the DrugBank database for 2018,” *Nucleic Acids Research,* 2018, doi: 10.1093/nar/gkx1037.

[179] R. A. Friesner et al., “Glide: A New Approach for Rapid, Accurate Docking and Scoring. 1. Method and Assessment of Docking Accuracy,” *Journal of Medicinal Chemistry,* 2004, doi: 10.1021/jm0306430.

[180] T. A. Halgren et al., “Glide: A New Approach for Rapid, Accurate Docking and Scoring. 2. Enrichment Factors in Database Screening,” *Journal of Medicinal Chemistry,* 2004, doi: 10.1021/jm030644s.

[181] R. A. Friesner et al., “Extra Precision Glide: Docking and Scoring Incorporating a Model of Hydrophobic Enclosure for Protein - Ligand Complexes,” *Journal of Medicinal Chemistry*, pp. 6177–6196, 2006.

[182] S. Kim, J. Lee, S. Jo, C. L. Brooks, H. S. Lee, and W. Im, “CHARMM-GUI ligand reader and modeler for CHARMM force field generation of small molecules,” *Journal of Computational Chemistry,* 2017, doi: 10.1002/jcc.24829.

[183] W. Humphrey, A. Dalke, and K. Schulten, “VMD: Visual molecular dynamics,” *Journal of Molecular Graphics,* 1996, doi: 10.1016/0263-7855(96)00018-5.

[184] J. Stone, “An Efficient Library for Parallel Ray Tracing and Animation*,” In Intel Supercomputer Users Group Proceedings,* 1995.

[185] M. J. Abraham et al., “GROMACS: High performance molecular simulations through multi-level parallelism from laptops to supercomputers,” *SoftwareX*, vol. 1–2, pp. 19–25, Sep. 2015, doi: 10.1016/J.SOFTX.2015.06.001.

[186] H. J. C. B. Emile Apol, Rossen Apostolov et al., “GROMACS User Manual.” 2016.

[187] C. J. Der, T. Finkel, and G. M. Cooper, “Biological and biochemical properties of human rasH genes mutated at codon 61,” *Cell*, 1986, doi: 10.1016/0092-8674(86)90495-2.

[188] F. Shima et al., “Structural basis for conformational dynamics of GTP-bound ras protein,” *Journal of Biological Chemistry*, 2010, doi: 10.1074/jbc.M110.125161.

[189] M. Araki et al., “Solution structure of the state 1 conformer of GTP-bound H-ras protein and distinct dynamic properties between the state 1 and state 2 conformers,” *Journal of Biological Chemistry*, 2011, doi: 10.1074/jbc.M111.227074.

[190] T. Liu, Y. Lin, X. Wen, R. N. Jorissen, and M. K. Gilson, “BindingDB: A web-accessible database of experimentally determined protein-ligand binding affinities,” *Nucleic Acids Research*, 2007, doi: 10.1093/nar/gkl999.

[191] M. Davies et al., “ChEMBL web services: Streamlining access to drug discovery data and utilities,” *Nucleic Acids Research*, 2015, doi: 10.1093/nar/gkv352.

[192] D. Mendez et al., “ChEMBL: Towards direct deposition of bioassay data,” *Nucleic Acids Research*, 2019, doi: 10.1093/nar/gky1075.

[193] Z. Zhang et al., “GTP-state-selective cyclic peptide ligands of K-ras(G12D) block its interaction with Raf,” *ACS Central Science*, 2020, doi: 10.1021/acscentsci.0c00514.

CURRICULUM VITAE

Name Surname : Metehan İlter

EDUCATION:

B.Sc. : 2019, İstanbul Medipol University, School of Engineering and Natural Sciences, Biomedical Engineering

PROFESSIONAL EXPERIENCE AND REWARDS:

- 2015-2016 Fall and Spring Semesters, High Honor Student, Istanbul Medipol University
- 2016-2017 Fall and Spring Semesters, High Honor Student, Istanbul Medipol University
- 2017-2018 Fall and Spring Semesters, High Honor Student, Istanbul Medipol University
- 2018, 2nd Best Poster Presentation at the 6th International Congres of Molecular Biology Association of Turkey, İzmir
- 2018-2019 Fall and Spring Semesters, High Honor Student, Istanbul Medipol University

PUBLICATIONS, PRESENTATIONS, AND PATENTS ON THE THESIS:

- M. Ilter and O. Sensoy, "Catalytically competent non-transforming H-RAS^{G12P} mutant provides insight into molecular switch function and GAP-independent GTPase activity of RAS," in *Scientific reports*, vol. 9, no. 1, *Nature Publishing Group*, 2019, pp. 1–10.
- M. Ilter, and O. Sensoy, "Impairing GTPase cycle of RAS via therapeutics: Alternative to SHP2 inhibitors used in cancer treatment," presented at the 7th International Congress of Molecular Biology Association of Turkey, İstanbul, Sept. 27–29, 2019.
- M. Ilter, and O. Sensoy, "Impairing GTPase cycle of RAS via therapeutics: Alternative to SHP2 inhibitors used in cancer treatment," in *Turkish Journal of Biology*, vol. 43, no 5 (Suppl), *The Scientific and Technological Research Council of Turkey*, 2019.
- M. Ilter, and O. Sensoy, "Modulating the interaction of H-RAS G12D mutant (H-RAS^{G12D}) with RAF with the help of small molecules: A repurposing study that unveils potential therapeutics for the treatment of thyroid neoplasm," presented at the International Max Planck Research School ProEng Selection Colloquium, Magdeburg/Germany, Dec. 18, 2020.

- M. Ilter, F. Jalalypour, C. Atılgan, and O. Sensoy, "Inhibiting H-RAS^{G12D}-RAF interaction by mimicking Src-kinase mediated phosphorylation," (Manuscript in preparation)

OTHER PUBLICATIONS, PRESENTATIONS, AND PATENTS:

- M. Ilter, and O. Sensoy, "Comparative analysis of structural and dynamic properties of transforming (H-RAS^{G12D}), non-transforming (H-RAS^{G12P}) and wild-type (H-RAS^{WT}) H-RAS protein," presented at the 6th International Congress of Molecular Biology Association of Turkey, İzmir, Sep. 5-8, 2018.
- M. Ilter, and O. Sensoy, "Comparative assessment of structural and dynamic properties of transforming (H-RAS^{G12D}) and non-transforming (H-RAS^{G12P})," presented at the 6th International BAU Drug Design Congress, İstanbul, Dec. 13-15, 2018.
- M. Ilter, S. Mansoor, and O. Sensoy, "Utilization of G protein-coupled receptor signaling towards development of safer and personalized therapeutics," in *Molecules*, vol. 24, no. 11, *Multidisciplinary Digital Publishing Institute*, 2019, pp. 2052.
- H. Pekel, M. Ilter and O. Sensoy, "SARS-Cov-2 ana proteaz enziminin katalitik aktivitesini inhibe edebilen küçük terapötik moleküller," Türk Patent ve Marka Kurumu 2020-GE-649526, Dec. 15, 2020
- H. Pekel, M. Ilter and O. Sensoy, "Inhibition of SARS-CoV-2 main protease: A repurposing study that targets the dimer interface of the protein," in *Journal of Biomolecular Structure and Dynamics, Taylor & Francis*, 2021, pp. 1–10.

UNDERSTANDING THE IMPACT OF PHOSPHORYLATION AND MEMBRANE ON STRUCTURE AND DYNAMICS OF RAS BY MEANS OF MOLECULAR DYNAMICS SIMULATIONS

ORIGINALITY REPORT

13%	9%	10%	3%
SIMILARITY INDEX	INTERNET SOURCES	PUBLICATIONS	STUDENT PAPERS

PRIMARY SOURCES

1	Sander Roet, Ferry Hooft, Peter G. Bolhuis, David W.H. Swenson, Jocelyne Vreede. "Path sampling simulations reveal how the Q61L mutation restricts the dynamics of KRas", Cold Spring Harbor Laboratory, 2020 Publication	1%
2	Submitted to Eastern Mediterranean University Student Paper	1%
3	www.mdpi.com Internet Source	<1%
4	Shaoyong Lu, Hyunbum Jang, Serena Muratcioglu, Attila Gursoy, Ozlem Keskin, Ruth Nussinov, Jian Zhang. "Ras Conformational Ensembles, Allostery, and Signaling", Chemical Reviews, 2016 Publication	<1%
5	Submitted to Nashville State Community College	<1%